TECHNISCHE UNIVERSITÄT WIEN

INSTITUT FÜR MECHANIK UND MECHATRONIK
Mechanics & Mechatronics

DIPLOMA THESIS

Torque Emulation for Teleoperated Vehicles

submitted in satisfaction of the requirements for the degree Diplom-Ingenieur (Dipl.-Ing. or DI) under the supervision of

Ao.Univ.Prof. Dipl.-Ing. Dr.techn. Manfred Plöchl
(Institute of Mechanics and Mechatronics, E325-01)

and

Dipl.-Ing. Dr. Mathias Metzler
(Vay Technology GmbH)

Submitted to the Vienna University of Technology
Faculty of Mechanical and Industrial Engineering

Ypti Hossain, BSc
11701209
(UE 066 445)

Affidavit

I declare in lieu of oath that this thesis has been prepared by me independently in accordance with the recognised principles for scientific papers. All aids used, especially the literature used as a basis, are mentioned and listed in this thesis. The passages taken verbatim from the sources are marked as such.

The topic of this thesis has not been presented by me in any form as an examination paper to an assessor in Austria or abroad. This work agrees with the work assessed by the assessors.

Vienna, September 2023 Ypti Hossain, BSc

Danksagung

Hiermit möchte ich mich bei allen bedanken, die mich beim Abschluss meiner Diplomarbeit unterstützt haben.

An erster Stelle möchte ich meinen Betreuern, Dr. Mathias Metzler, Prof. Manfred Plöchl und Prof. Johannes Edelmann, meinen tiefsten Dank aussprechen. Ihre Anleitung, Unterstützung und wertvollen Ratschläge haben maßgeblich zur Gestaltung dieser Arbeit beigetragen. Sie hatten jederzeit ein offenes Ohr für meine Anliegen, und ihre Ratschläge haben maßgeblich zu meiner fachlichen und persönlichen Entwicklung beigetragen.

Ebenfalls möchte ich mich bei dem Unternehmen und allen Mitarbeitern von Vay Technology herzlich für die großartige Zusammenarbeit bedanken. Darüber hinaus möchte ich mich bei allen Mitarbeitern des Instituts für Mechanik und Mechatronik bedanken, und ganz besonders bei Philipp Mandl, der mir die benötigte Ausrüstung zur Verfügung gestellt und mich beim Einrichten dieser unterstützt hat.

Schließlich möchte ich meiner Familie und meinen Freunden für ihre fortwährende Unterstützung und ihr Verständnis während dieser anspruchsvollen Zeit danken. Besonderer Dank geht an meine Mutter, meine Lebensgefährtin und meine Schwester. Ihr Glaube an mich hat mich motiviert und nur durch ihre Unterstützung konnte ich mein Studium erfolgreich abschließen.

Acknowledgements

I would like to express my gratitude to all those who supported me in completing my diploma thesis.

First and foremost, I want to extend my deepest thanks to my supervisors, Dr. Mathias Metzler, Prof. Manfred Plöchl, and Prof. Johannes Edelmann. Their guidance, support, and valuable advices significantly contributed to shaping this work. They were always available to address my concerns, and their advice played an important role in my professional and personal development.

I would also like to express my sincere gratitude to the company Vay Technology and all the employees for their outstanding collaboration. Furthermore, I would like to thank all the staff members at the Institute of Mechanics and especially Philipp Mandl, for providing me with the necessary equipment and assisting me during the set-up.

Finally, I would like to thank my family and friends for their continuous support and understanding during this challenging period. Special thanks go to my mother, my partner, and my sister. Their belief in me motivated me, and it is thanks to their support that I successfully completed my studies.

Kurzfassung

Teleoperierte Fahrzeuge gewinnen zunehmend an Bedeutung, da nach dem aktuellen Stand der Entwicklung automatisierte Fahrzeuge nicht in der Lage sind in allen Umgebungen und unter allen Bedingungen zu operieren. Trotz des großen Potenzials der teleoperierten Fahrzeuge bestehen noch einige zu lösende Herausforderungen. Da der Fahrer beim Teleoperieren eines Fahrzeugs nicht physisch im Fahrzeug anwesend ist, fehlt ihm die unmittelbare Wahrnehmung des Fahrzeugs. Diese Arbeit beleuchtet die Unterschiede zwischen dem Telefahren und dem gewöhnlichen Alltagsfahren aus der theoretischen Perspektive. Zudem wird der Einfluss der Totzeit zufolge der Signalübertragung und der fehlenden Wahrnehmung des Fahrzeugs auf die Stabilität des teleoperierten Fahrzeug-Telefahrer-Systems untersucht. Um die Wahrnehmung des Fahrers und die Steuerbarkeit des teleoperierten Fahrzeugs zu erhöhen, wird ein Konzept für die Lenkmomentenemulation entwickelt. Dieses Konzept weist eine einfache Struktur auf, die bei Bedarf angepasst werden. Der Vorteil bei dieser einfachen Struktur ist die Möglichkeit der Echtzeitberechnung. Zur Berechnung den Lenkmoments wird neben dem Lenkwinkel und der Lenkwinkelrate des Telefahrers, die Querbeschleunigung und die Gierrate des Fahrzeugs herangezogen. Es werden verschiedenen Lenkmomentenemulation-Modi erarbeitet, um ihren Einfluss auf das Lenkverhalten des Telefahrers zu untersuchen. Zum Testen dieser Lenkmomentenemulation-Modi in einer geschützten Umgebung wurde ein Tele-Fahrsimulator entwickelt. Dieser wurde in Zusammenarbeit mit dem Unternehmen Vay an die reale Telestation von Vay abgestimmt. Nach den Untersuchungen im Simulator wird die Lenkmomentenemulationskomponente in die echte Telestation integriert. Die Ergebnisse der Tests sowohl am Simulator als auch an der realen Telestation zeigen, dass das vorgeschlagene Konzept der Lenkmomentenemulation den Telefahrern das Lenken des teleoperierten Fahrzeugs erleichtert und dabei unterstützt das Fahrzeug stabil zu lenken.

Abstract

Teleoperated vehicles are gaining importance during the transition to fully automated vehicles since at the current state of development automated vehicles are not capable of operating in all conditions and environments. Despite the high potential of the concept of teleoperated vehicles, there are still challenges to be dealt with. As the driver is not physically present in the vehicle when teleoperating a vehicle, they lack information about the vehicle motion. This study demonstrates from a theoretical perspective the differences between teledriving and normal driving and how the stability of the teleoperated vehicle-teledriver system is affected by the communication delay and the missing perception of the vehicle. To increase the driver's perception and the manoeuvrability of the teleoperated vehicle, a simple structured, tunable torque emulation concept is introduced. Due to the simple structure of the torque emulation component, the calculation can be executed in real-time. The torque emulation concept utilises the teledriver's steering angle, steering wheel angle rate, and the vehicle's states, such as lateral acceleration and yaw rate, to generate a steering wheel feedback torque. To test the different torque emulation modes a teledriving simulator is developed. As a collaboration with the company Vay, the simulator is parametrised to have the same behaviour as the real telestation of Vay. Before implementing the torque emulation component into the real telestation, the teledriving simulator is used as a safe environment for testing the influence of the torque feedback. The results of the tests at both the simulator and real telestation demonstrate that the proposed torque emulation concept assists teledrivers in steering the vehicle in a stable fashion and eases the steering task.

Contents

1. Introduction

In recent years autonomous driving has become a focal point of research and development. Unfortunately, there is currently no automated vehicle that is capable of operating in all conditions and environments, as defined in SAE [1] level 5. Automated vehicles still require human intervention in unknown driving environments or the event of hardware or software failure. As a transition to fully automated vehicles, teledriving, also known as remote operation, of vehicles over the internet plays an important role. Teleoperated vehicles can be employed in various practical scenarios, including taxi services, delivery services [2], and shared mobility platforms [3]. In shared mobility settings, a teledriver could take over tasks such as picking up the vehicle from specific locations or searching parking spots [3].

The main advantage of teleoperated vehicles is that the human driver remains in the vehicle control loop. The driver can operate the vehicle without the need for high-precision maps and can respond to critical situations that an autonomous vehicle may not have been trained for [4]. Despite the high potential of the concept of teleoperated vehicles, there are still challenges in its realisation. The control signals of the teledriver such as steering input, throttle, and brake pedal positions are transmitted to the vehicle control unit (VCU) over the internet and thus the signal transmission is delayed. To provide the teledriver with appropriate visual and acoustic feedback, the teleoperated vehicle has to be equipped with cameras and speakers. Likewise, there is a time delay for these signals to reach the telestation [5]. In Figure 1.1 the schematic structure of the telestation and the teleoperated vehicle is illustrated.

Despite the high potential of the concept of teleoperated vehicles, there are still challenges to be dealt with. As the driver is not physically present in the vehicle when teleoperating a vehicle, they lack information about the vehicle motion. Being physically present in the vehicle provides the driver with the information of the velocity, acceleration, and an immediate steering torque feedback. The steering torque feedback is often referred to as the steering feel. It influences the driver's perception and the manoeuvrability of a vehicle [6]. The steering feel is a crucial characteristic for evaluating the driving behaviour of a vehicle. It serves as an information source for the driver

regarding the tire-road contact and vehicle's states. When the information is transmitted to the driver as haptic feedback, they can react faster to changing road conditions and vehicle states compared to sole visual feedback [7]. As there is no physical contact between the steering system of the telestation and the vehicle, the steering torque has to be emulated to increase the teledriver's steering feel.

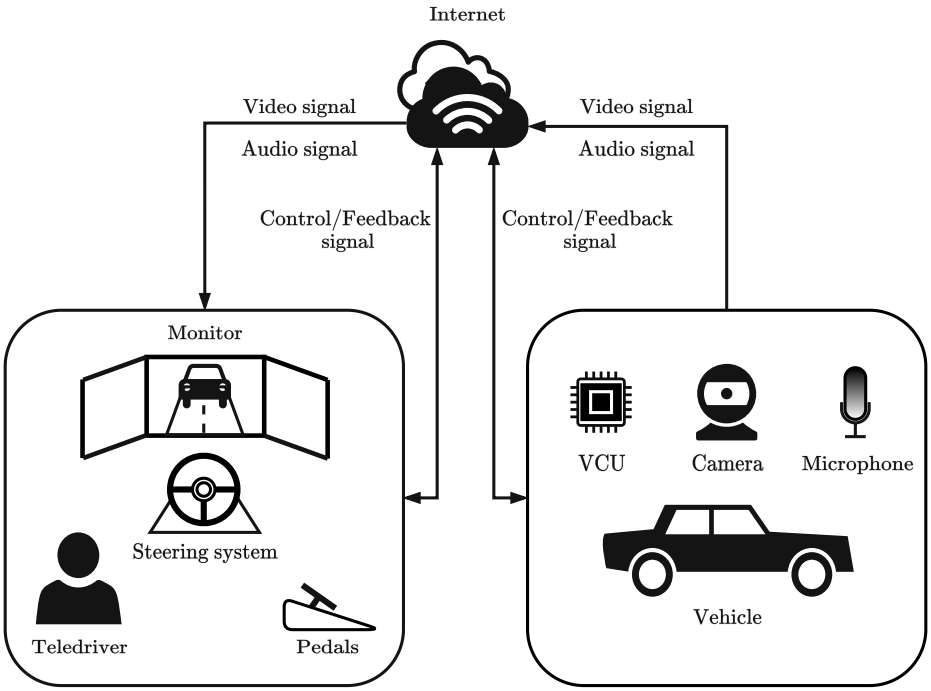

Figure 1.1.: Teleoperated vehicle system based on [5]

1.1. Objective

The objective of this diploma thesis is to provide a comprehensive analysis of torque emulation for teleoperated vehicles. The torque emulation concept is developed based on the teledriver inputs and the vehicle's states. Moreover, the concept offer a straightforward structure that can be easily adapted to suit various preferences and steering systems. To test the different torque emulation modes under the influence of the communication time delay, a teledriving simulator is developed. The teledriving simulator is used as a safe environment for testing the influence of the torque feedback before implementing the torque emulation component into the real telestation. Furthermore, it provides an investigation into how the communication time delay and the absence of perception in-

fluence the stability of the teleoperated vehicle-teledriver system. Therefore, a teledriver model is introduced.

1.2. Literature Review

In the literature, there are different approaches to steering torque feedback based on the steering system. In a vehicle with Electric Power Steering (EPS), the steering of the vehicle is supported by an electric motor. The goals of an EPS system are to make driving easier, more comfortable, and safer. In addition, the EPS system transfers a portion of the EPS torque to the steering column to provide the driver with feedback on the interaction between the tire and the road [6]. EPS assist torques typically rely on characteristic curves, that are also referred as to boost curves. These boost curves often depend on torque measurements at the torsion bar, and the velocity [8][9][10]. Some of the literature proposes a torque that the driver should feel, known as reference torque, based on the steering wheel angle and the vehicle's longitudinal velocity in the form of a torque map [11]. Others include the steering wheel angle rate [12] and the lateral acceleration [13][14] to the torque map and develop the assist torque based on it.

In Steer-by-Wire (SBW) systems, there is no physical coupling between the steering column and steering rack. The desired steering angle from the driver is transmitted from the vehicle's communication system to the steering system. The steering feedback torque can be designed freely to provide the driver with a realistic or improved artificial steering feel [15]. In [16], an artificial feedback based on mathematical models for the aligning torque, jacking torque, and damping torque is proposed. However, the aligning torque, and jacking torque, need extensive tire information due to the numerous parameters in the model.

In [17], Fankem and Müller propose a modular steering torque generation for driving simulators and SBW systems that can be tuned to achieve the desired steering feel. The main part of the feedback torque is based on the steering rack force and the vehicle's longitudinal velocity. In addition, friction torque, damping torque, inertia torque and active return torque are calculated based on the steering wheel angle and the steering wheel angle rate. For the active return torque, the measurement of the applied torque on the steering wheel is utilised. Despite the simple structure of the torque emulation, the primary challenge lies in the accurate estimation of the rack force. Therefore, a steering

system model based rack force estimation is proposed in [18]. Furthermore, a vehicle-tire model based method for rack force estimation is presented in [6]. The accuracy of these approaches depends heavily on the knowledge of the parameters of the steering system and the tire. Koch uses rack force measurements to emulate the steering wheel torque [7]. This method might lead to very good results in terms of a realistic steering feel. Nevertheless, the measurement of the rack force is not available in every vehicle and measurement costs are too high to be feasible in production vehicles.

The steering of a teleoperated vehicle is very similar to the steering of a vehicle with a Steer-by-Wire function. The difference lies only in the communication and the resulting delays in signal transmission. In [5], a steering system model is used to estimate the self aligning torque with a non linear disturbance observer. Moreover, a friction torque based on steering pinion angular velocity is considered. To adjust the feedback torque, a weighting function dependent on the steering wheel angle is proposed. This approach provides a simple structure but still requires a profound knowledge of the steering system parameters.

2. Teledriving

2.1. Driver Model

Before analysing the teledriver characteristics, the regular driver model with a normal vehicle should be investigated first. The closed-loop model of a vehicle-driver system can be modelled as shown in Figure 2.1.

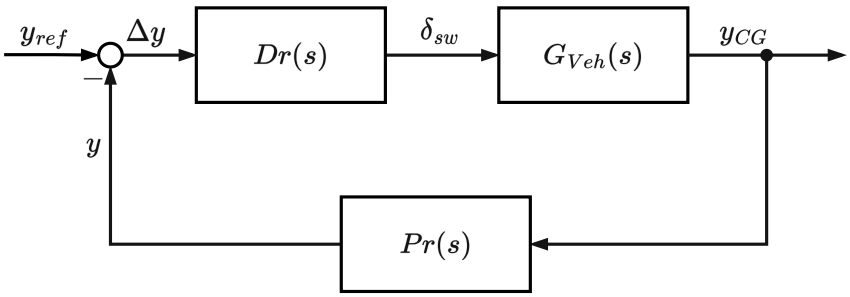

Figure 2.1.: Block diagram of the vehicle-driver system

As described in [19], the vehicle-driver system consists of the vehicle $G_{Veh}(s)$, the driver $Dr(s)$ and a prediction transfer function $Pr(s)$. A simple model to describe human driving behaviour is the Precision Model by McRuer [20]. The linear driver model is a simple transfer function with proportional-derivative (PD) behaviour:

$$Dr(s) = \frac{\delta_{sw}(s)}{\Delta y(s)} = K_{Dr}\frac{1+T_v s}{1+T_n s}e^{-T_R s} \tag{2.1}$$

The driver gain is denoted as K_{Dr}, T_v is the lead time and T_n is the lag time. The time delay T_R in the transfer function (2.1) describes the reaction time of the driver. Usually, the value of the reaction time is set to 0.2 s. The driver does not respond to the current deviation from the reference trajectory. In general, the driver looks ahead in the driving direction and estimates the deviation at a previewed point P and attempts to correct it. Therefore, the prediction transfer function $Pr(s)$ is included. The prediction transfer function takes the current lateral position $y_{CG}(t)$ and predicts the lateral position $y_{CG}(t+T_P)$. The preview time T_P is set to 0.084 s [19].

The prediction at preview time can be evaluated with Taylor series expansion as described in [19]:

$$y_{CG}(t+T_P) = y \approx y_{CG}(t) + \dot{y}_{CG}(t)T_P + \ddot{y}_{CG}(t)\frac{T_P^2}{2} \tag{2.2}$$

After Laplace-transformation we get:

$$Pr(s) = \frac{y(s)}{y_{CG}(s)} = e^{T_P s} \approx 1 + T_P s + \frac{T_P^2}{2}s^2 \tag{2.3}$$

The vehicle is modelled by the bicycle model with linear tire characteristics as shown in Figure 3.10. The transfer function has the following structure [21]:

$$G_{Veh}(s) = \frac{y_{CG}(s)}{\delta_{sw}(s)} = \frac{v_x}{i_L}\frac{G_r(s)/s + G_\beta(s)}{s} \tag{2.4}$$

The longitudinal velocity is denoted with v_x, the steering ratio with i_L, the yaw rate transfer function with $G_r(s)$ and the vehicle side slip angle transfer function with $G_\beta(s)$. A detailed derivation of the transfer functions and the vehicle parameters is given in Section 3.4.

To identify the parameters of the driver model, the open-loop system is analysed. Mitschke describes in [19] some criteria for the calculation of the driver model parameters given in Equation 2.1:

- The crossover frequency should range from $\omega_c = 0.1\,\text{Hz}$ (normal driving situation) to $\omega_c = 0.7\,\text{Hz}$ (critical driving situation).
- The usual phase margin φ_R of a driver ranges from $30\,^\circ$ to $50\,^\circ$.
- The slope of the open-loop amplitude response should be around $-20\,\text{dB/dec}$ near the crossover frequency ω_c. That allows the conclusion on the closed-loop system from the open-loop system.

Generally, the driver adapts his parameters, without changing the structure of the driver transfer function (2.1), to the vehicle in such a way that the relationship in Equation 2.5 holds true around the crossover frequency. That shows that the driver is able to operate different vehicles at different velocities, and driving conditions [19].

$$G_o(s) = Dr(s)G_{Veh}(s)Pr(s) = const. = \frac{\omega_c}{s}e^{-T_R s} \tag{2.5}$$

In addition to the phase margin $\varphi_R = 30°$, the damping ratio ζ and the settling time T_{ar} for reaching the $\Delta 5\,\%$ range of the reference input are chosen to define the dynamic specifications. These specifications define how the driver controls the system. The damping ratio $\zeta = 1/\sqrt{2}$ and the settling time $T_{ar} = 1.7\,\mathrm{s}$ as suggested in [22][23]. The specifications lead to the desired closed-loop transfer function. Detailed calculation of T is given in [22]:

$$G_{w,des}(s) = \frac{y_{CG}(s)}{y_{ref}(s)} = \frac{1}{1 + 2\zeta T s + T^2 s^2} \tag{2.6}$$

Accordingly, the desired open-loop transfer function is:

$$G_{o,des}(s) = \frac{y(s)}{y_{ref}(s)} = \frac{1}{2\zeta T s + T^2 s^2} \tag{2.7}$$

A Matlab script is used to determine the driver model parameters. The desired crossover frequency is determined from the desired open-loop transfer function and is 0.285 Hz. With the desired crossover frequency and the desired phase margin $\varphi_R = 30°$ the vehicle parameters K_{Dr}, T_v and T_n are evaluated as described in [24]. In the Table 2.1 the parameters of a regular driver are given.

v_x	K_{Dr}	T_v	T_n
30 km/h	0.865 rad/m	1.071 s	0.292 s

Table 2.1.: Parameters of a regular driver

2.2. Teledriver Model

In this chapter, the behaviour of the teledriver, and the behaviour of a regular driver operating a vehicle remotely are investigated. When the driver is not physically present in the vehicle, the communication between the driver and the vehicle takes place via the Internet. That leads to a delay not only in the telemetry signals but also in the transmission of the visual signal. The delay is determined by measuring the time it takes for a signal to be sent by the host and received back. This measured time is referred to as the round-trip time (RTT) and half of the RTT is the communication time delay T_C. The communication time delay depends on the network quality and usually contains nondeterministic fluctuations known as jitter [25].

However, for the purposes of this investigation, the communication delay time is assumed to be constant. In the Figure 2.2, the block diagram of the teleoperated vehicle-teledriver system is shown. The driver inputs are transmitted to the vehicle with a communication delay. The vehicle's output and the visual information are transmitted to the driver with a communication delay as well. Therefore, the delay block $G_{Com}(s)$ is added.

$$G_{Com}(s) = e^{-T_C s} \tag{2.8}$$

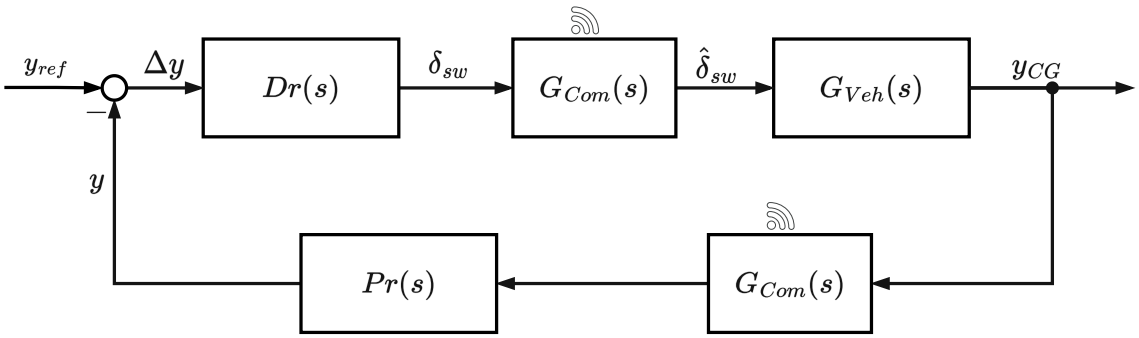

Figure 2.2.: Block diagram of the teleoperated vehicle-teledriver system

2.2.1. Influence of the Communication Delay

In this section, the influence of time delay on human driving behaviour is investigated. Therefore, the parameters of a driver, who has no knowledge of the additional communication delay, are calculated. It should be noted that the driver is fully aware of the changing velocity and the states of the vehicle and adapts his parameters to satisfy the Equation 2.5. It is the same as if a regular driver is operating the vehicle remotely, but without being aware of it. The open-loop transfer function of the teleoperated vehicle with a regular driver is given below:

$$G_{o,TS}(s) = Dr(s)G_{Com}(s)G_{Veh}(s)G_{Com}(s)Pr(s) \tag{2.9}$$

The driver parameters are taken from the Table 2.1 in Section 2.1. The additional time delay in the system has the effect of increasing reaction time and decreasing preview.

$$Dr(s)G_{Com}(s) = K_{Dr}\frac{1+T_v s}{1+T_n s}e^{-(T_R+T_C)s} \tag{2.10}$$

$$Pr(s)G_{Com}(s) = e^{T_P s}e^{-T_C s} \approx \left(1 + T_P s + \frac{T_P^2}{2}s^2\right)e^{-T_C s} \tag{2.11}$$

The stability of the closed-loop system is evaluated based on the Nyquist stability criterion. For closed-loop stability, the phase of the open-loop system should be greater than $-180°$ at the crossover frequency ω_c and the phase margin φ_R has to be greater than 0, respectively [22]. The amplitude and the phase response of the open-loop transfer function at $v_x = 30\,\text{km/h}$ with varying communication delay time T_C are plotted in Figure 2.3, and Figure 2.4.

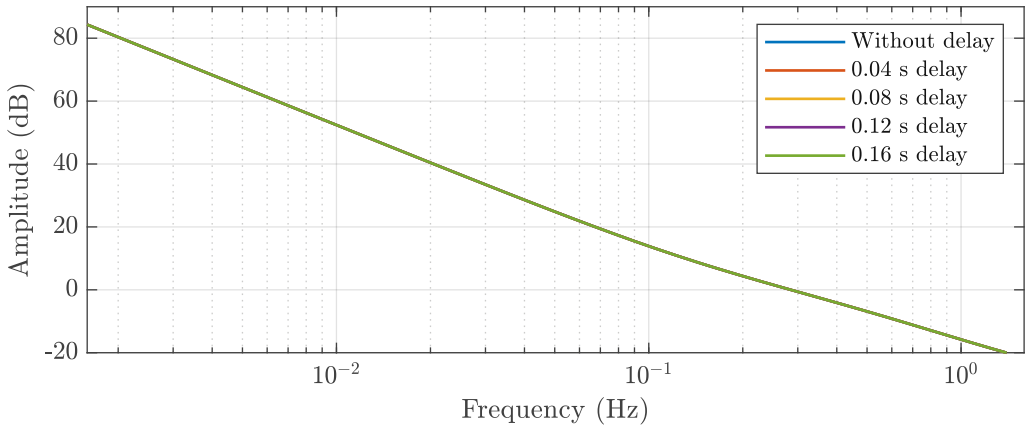

Figure 2.3.: Amplitude response of the open-loop transfer function $G_{o,TS}(s)$ at $v_x = 30\,\text{km/h}$ with varying time delay T_C

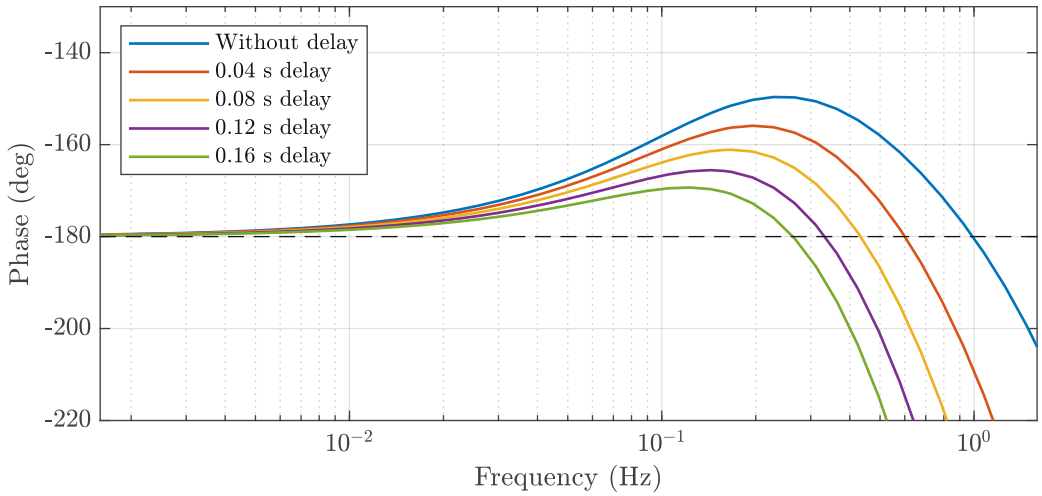

Figure 2.4.: Phase response of the open-loop transfer function $G_{o,TS}(s)$ at $v_x = 30\,\text{km/h}$ with varying time delay T_C

With increasing delay time, the phase margin decreases. The amplitude response is not

influenced by the time delay and thus the crossover frequency does not change as shown in Table 2.2. As the phase margin is negative at $T_C = 0.16\,\mathrm{s}$ the closed-loop system is unstable. The system is marginally stable at $T_C = 0.146\,\mathrm{s}$.

T_C	φ_R	ω_c
0 s	30.00 °	0.285 Hz
0.04 s	21.80 °	0.285 Hz
0.08 s	13.59 °	0.285 Hz
0.12 s	5.39 °	0.285 Hz
0.16 s	−2.82 °	0.285 Hz

Table 2.2.: Influence of the time delay on the system stability

The amplitude and the phase of the communication delay is:

$$|G_{Com}(j\omega)| = 1, \quad \varphi_{G_{Com}}(\omega) = arg G_{Com}(j\omega) = -\omega T_C \tag{2.12}$$

The change of the phase response of the system at the crossover frequency ω_c in comparison to the system without communication delay is as follows:

$$\Delta\varphi_R = -2\omega_c T_C \tag{2.13}$$

In the Figure 2.5, the closed-loop system response to a ramp input is shown. This could be seen as a manoeuvre to avoid an obstacle. The closed-loop transfer function is evaluated as follows:

$$G_{w,TS}(s) = \frac{Dr(s)G_{Com}(s)G_{Veh}(s)}{1 + Dr(s)G_{Com}(s)G_{Veh}G_{Com}(s)(s)Pr(s)} = \frac{Dr(s)G_{Com}(s)G_{Veh}(s)}{1 + G_{o,TS}(s)} \tag{2.14}$$

The regular driver in a regular vehicle follows the reference trajectory with less overshoot than a regular driver in a teleoperated vehicle. Even though the system is not unstable at $T_C = 0.12\,\mathrm{s}$ in the sense of control theory, it can be said that for a phase margin $\varphi_R < 10\,^\circ$ the driver oscillates more and needs longer to reach the $\Delta 5\,\%$ range of the reference. High oscillations while following the reference trajectory might lead to an accident in the case of obstacle avoidance. As mentioned above the closed-loop system is clearly unstable at $T_C = 0.16\,\mathrm{s}$.

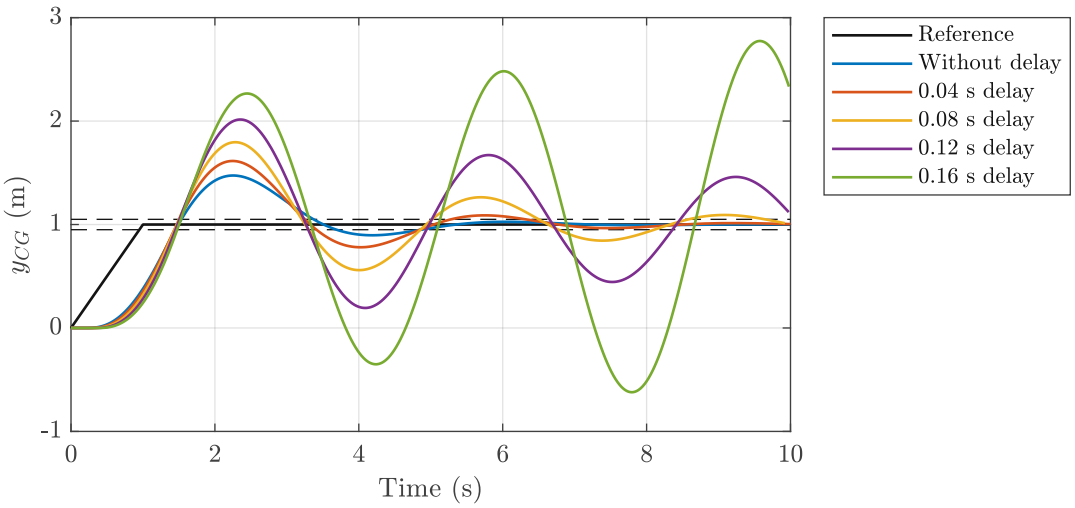

Figure 2.5.: Ramp response of the closed-loop system at $v_x = 30\,\mathrm{km/h}$ with varying time delay T_C

In the Figure 2.6 the delayed steering wheel angle is shown. It can be seen that the driver inputs are transmitted later and the amplitudes are higher with increasing time delay. The unstable system behaviour can be seen at $T_C = 0.16\,\mathrm{s}$.

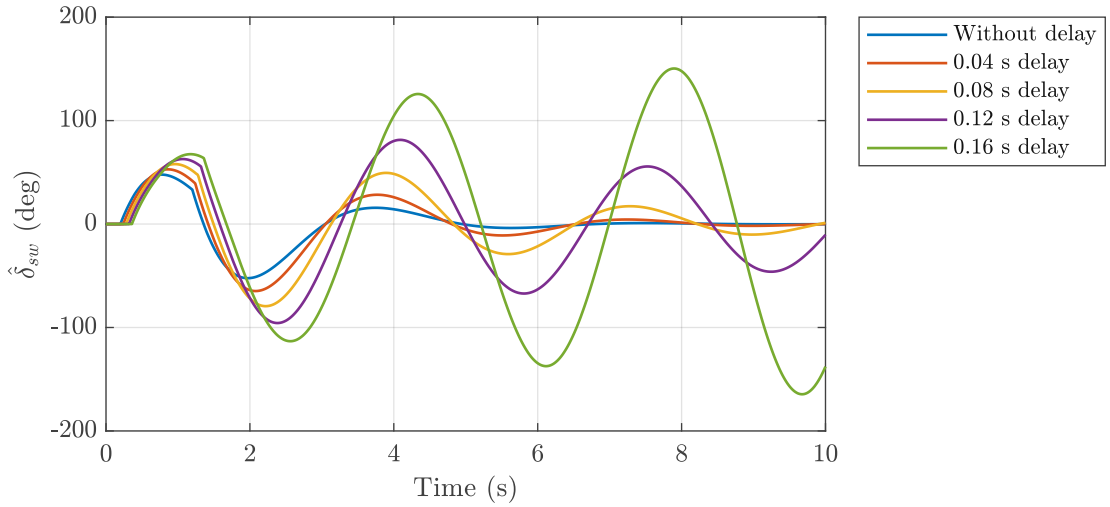

Figure 2.6.: Steering wheel input with varying time delay T_C

In the Figures 2.7 and 2.8, the vehicle's lateral acceleration and the yaw rate for different communication time delay are plotted.

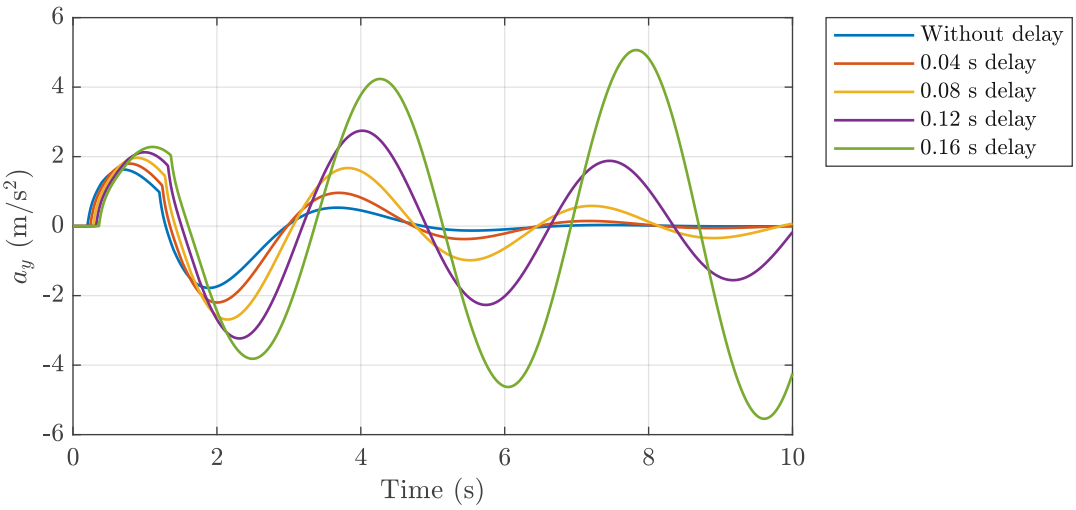

Figure 2.7.: Lateral acceleration with varying time delay T_C

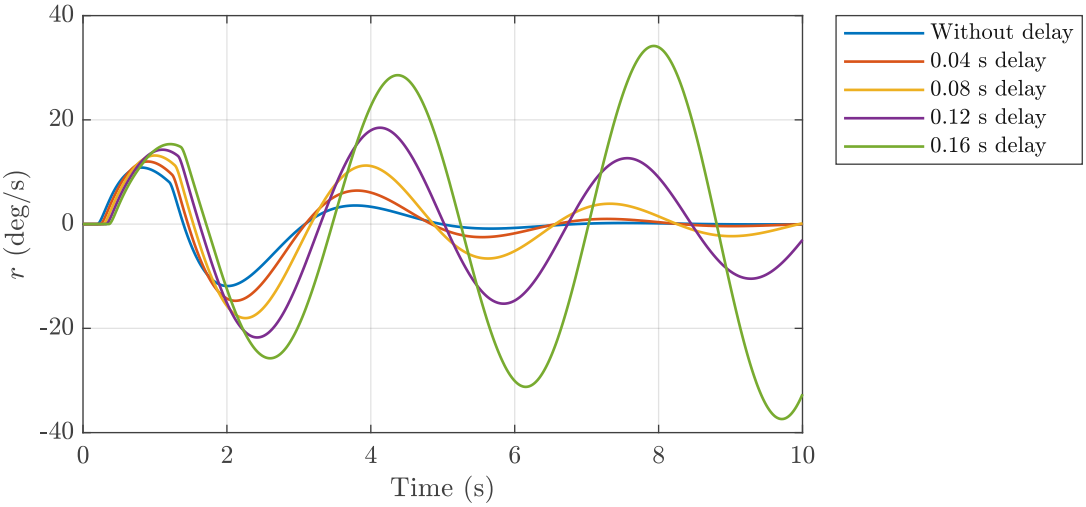

Figure 2.8.: Yaw rate with varying time delay T_C

2.2.2. Influence of the missing Perception

In this section, the influence of the missing perception in a teleoperated vehicle-teledriver system is discussed. Therefore, the parameters of a teledriver $\hat{Dr}(s)$ who knows how to drive the teleoperated vehicle with communication delay at a certain velocity are evaluated. Since the driver is not physically present in the vehicle, they lack information about the vehicle's states. Hence, they fail to adjust themselves to the changing vehicle behaviour as the velocity changes.

For the purposes of this investigation, the parameters of a teledriver, who can drive a teleoperated vehicle at $v_x = 30\,\mathrm{km/h}$ and with $T_C = 0.04\,\mathrm{s}$ are evaluated.

$$\hat{Dr}(s) = Dr(s)G_{Com}(s) = \frac{\hat{\delta}_{sw}(s)}{\Delta y(s)} = K_{Dr}\frac{1+T_v s}{1+T_n s}e^{-(T_R+T_C)s} \tag{2.15}$$

The driver parameters of the teledriver are given below:

v_x	K_{Dr}	T_v	T_n
30 km/h	0.719 rad/m	1.288 s	0.242 s

Table 2.3.: Parameters of a teledriver

In comparison to the parameters of a regular driver in Table 2.1, the driver gain K_{Dr} and the lag time T_n decrease and the lead time T_v increases. It should be noted that the teledriver is aware of the delayed visual information that he receives.

$$\hat{Pr}(s) = Pr(s)G_{Com}(s) \approx \left(1 + T_P s + \frac{T_P^2}{2}s^2\right)e^{-T_C s} \tag{2.16}$$

The open-loop transfer function of the teleoperated vehicle with a teledriver is given below:

$$\hat{G}_{o,TS}(s) = \hat{Dr}(s)G_{Veh}(s)\hat{Pr}(s) \tag{2.17}$$

The closed-loop transfer function of the teleoperated vehicle with a teledriver is similar to Equation 2.14:

$$\hat{G}_{w,TS}(s) = \frac{\hat{Dr}(s)G_{Veh}(s)}{1+\hat{Dr}(s)G_{Veh}(s)\hat{Pr}(s)}) = \frac{\hat{Dr}(s)G_{Veh}(s)}{1+\hat{G}_{o,TS}(s)} \tag{2.18}$$

In the following, the amplitude and phase response of the open-loop transfer function (2.17) are plotted in Figure 2.9 and Figure 2.10. As stated before, the vehicle's velocity is changed, but the teledriver can not adapt himself to it. It can be seen that the crossover frequency shifts to higher values with increasing velocity. In addition, the phase drop starts at a lower frequency with increasing velocity.

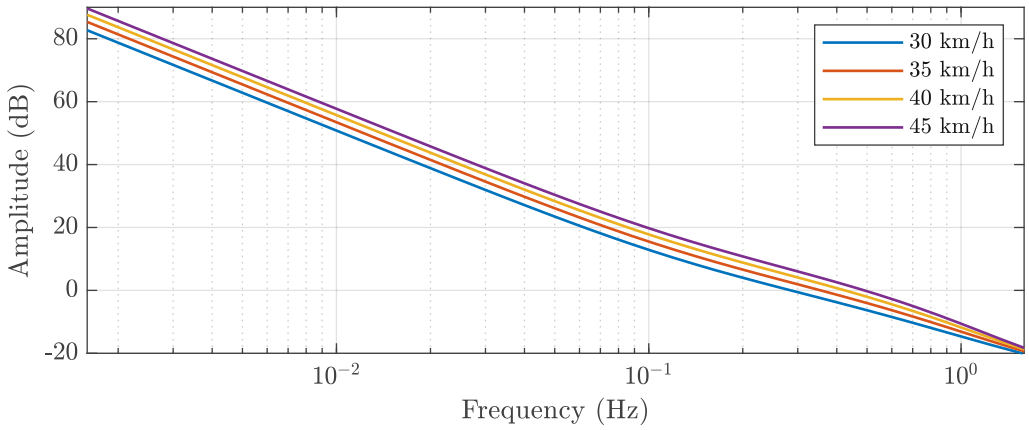

Figure 2.9.: Amplitude response of the open-loop transfer function $\hat{G}_{o,TS}(s)$ with a teledriver at different velocities

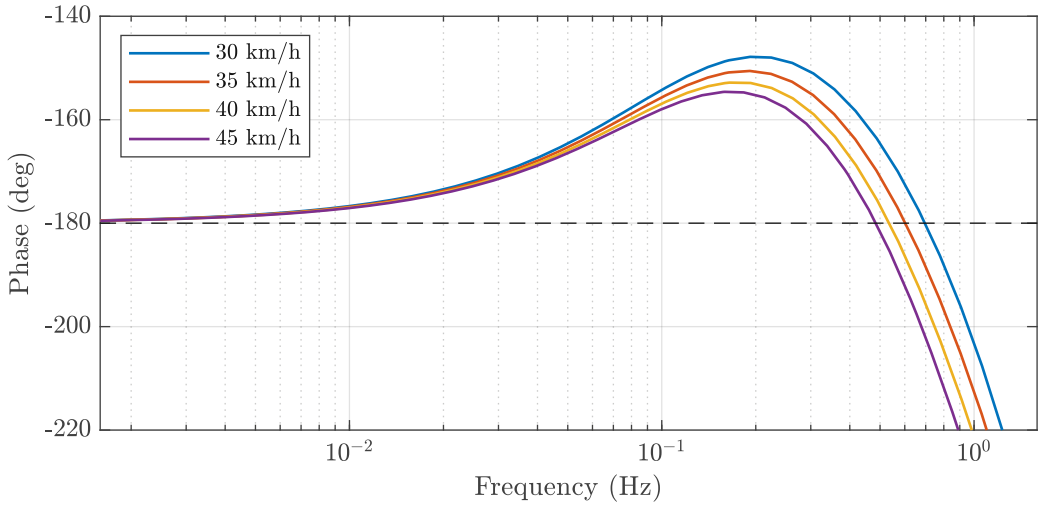

Figure 2.10.: Phase response of the open-loop transfer function $\hat{G}_{o,TS}(s)$ with a teledriver at different velocities

v_x	φ_R	ω_c
30 km/h	30.00 °	0.285 Hz
35 km/h	21.14 °	0.355 Hz
40 km/h	10.60 °	0.424 Hz
45 km/h	−0.62 °	0.490 Hz

Table 2.4.: Influence of the missing perception on the system stability

The values of the crossover frequency and the phase margin are summarised in the Table

2.4. The closed-loop system with the teledriver is unstable at 45 km/h and marginally stable at 44.7 km/h due to the missing perception. The closed-loop response to a ramp input shows the described effects in Figure 2.11. Specifically, when the teledriver operates at 40 km/h, it takes significantly more time to reach the 5 % of the reference trajectory. The amplitude increases with increasing velocity. This might lead to an accident in the case of obstacle avoidance.

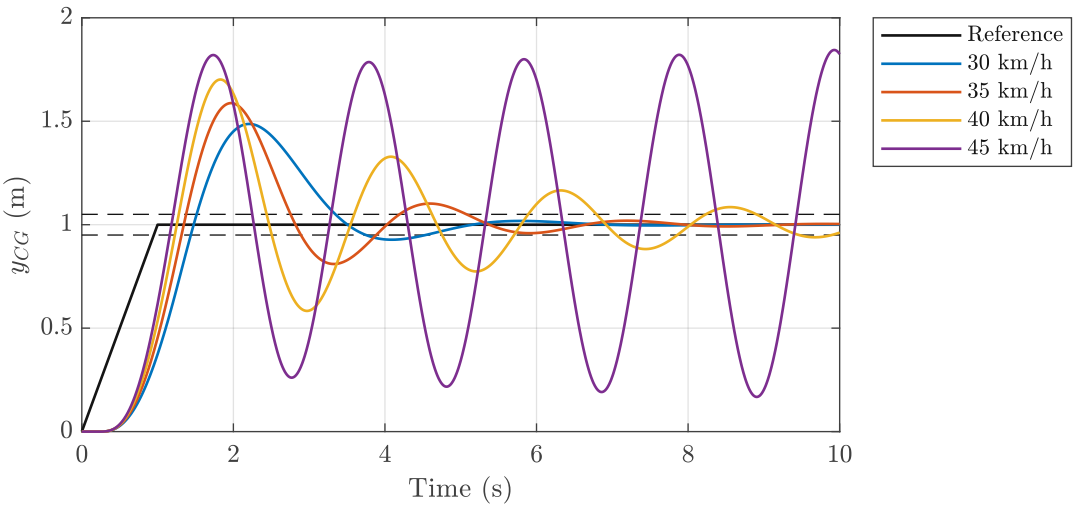

Figure 2.11.: Ramp response of the closed-loop system with a teledriver, and varying velocity v_x

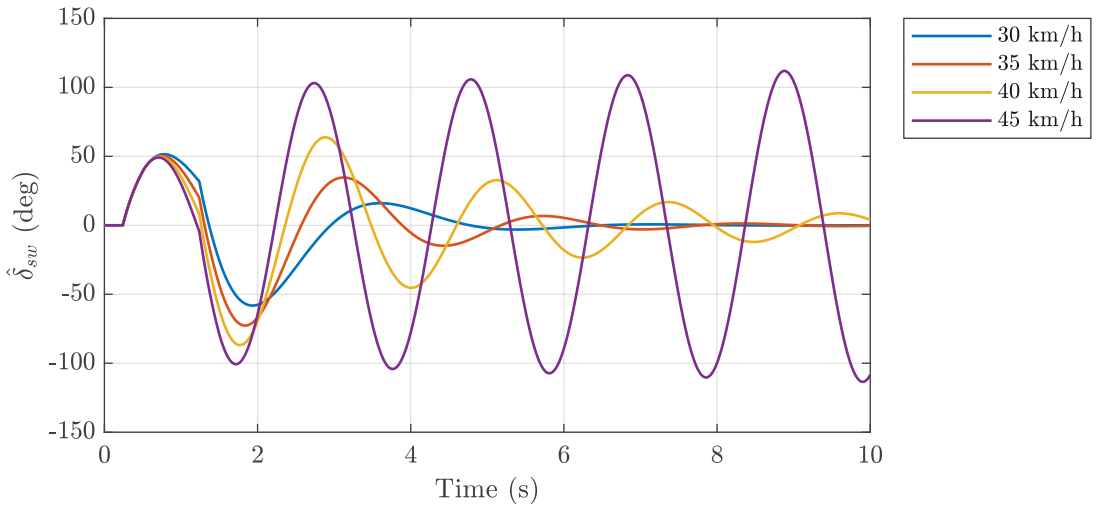

Figure 2.12.: Steering wheel input with varying velocity v_x

The steering angle inputs to the teleoperated vehicle are plotted in Figure 2.12. As the driver can not adapt to the vehicle, they steer more and more with increasing velocity,

until the system gets unstable. Furthermore, Figures 2.13 and 2.14 show the vehicle's lateral acceleration and the yaw rate for different velocities.

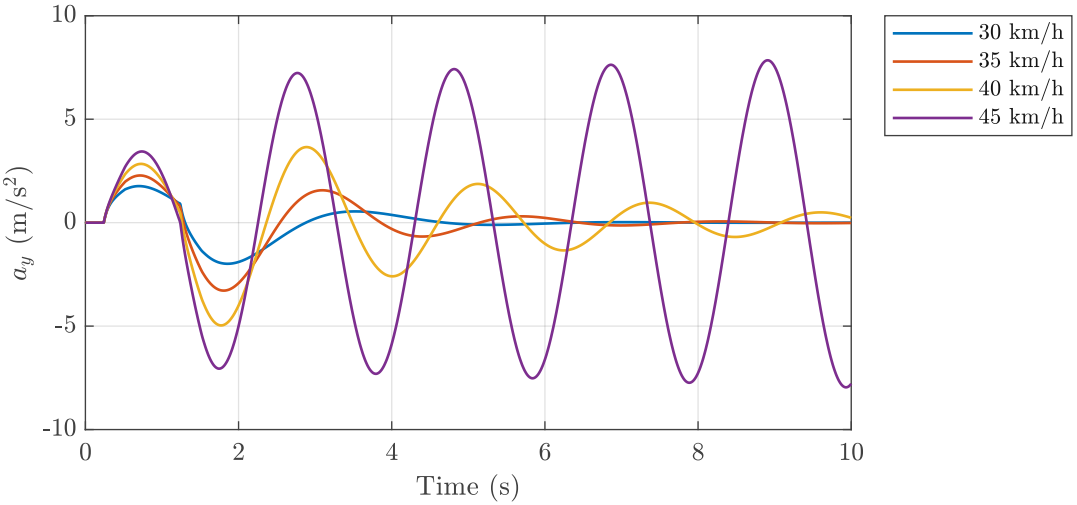

Figure 2.13.: Lateral acceleration with varying velocity v_x

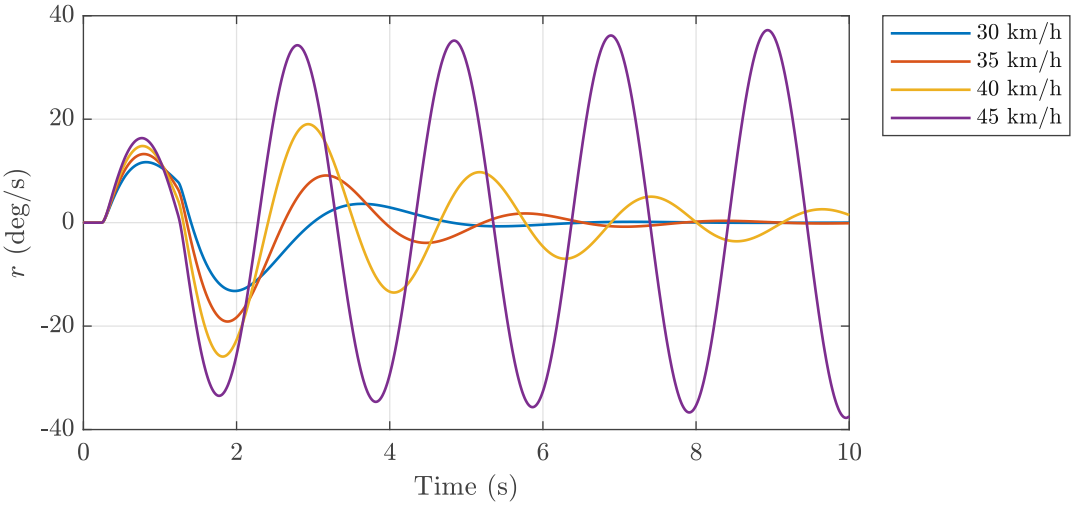

Figure 2.14.: Yaw rate with varying velocity v_x

As shown above, a teledriver might steer the vehicle with certain time delay and at a certain velocity, such as at 30 km/h, in a stable fashion. However, they might have difficulties adapting themselves to increasing velocities. This might lead to an unstable system. There might be teledrivers who can change their driver parameters, but still be unstable due to the communication time delay. In general, the teledriver has to cope with the influences of the time delay and the missing perception. It has been

shown that both can affect stability and it is the combination of these two effects that makes the teleoperation of a vehicle a challenging task. To increase the stability of the teleoperated vehicle-teledriver system, a phase-boosting element could be introduced that also increases the perception of the vehicle. However, the further development of the teleoperated vehicle-teledriver system model is beyond the scope of this study.

3. Teledriving Simulator

In this chapter, the development of the teledriving simulator is described. The aim is to develop a teledriving simulator that behaves like a real telestation. As reference, the telestation of Vay is chosen. In the Figure 3.1 the teledriving simulator is illustrated.

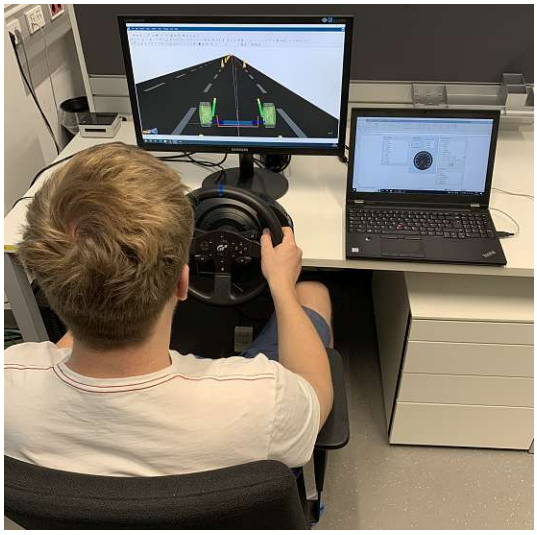

Figure 3.1.: Teledriving simulator

As shown in Figure 3.2, the real telestation has some additional features such as audio feedback, visualisation of the predicted trajectory and multiple camera views. The implementation of these additional features is beyond the scope of this study.

Figure 3.2.: Telestation of Vay

The teledriving simulator is used as a safe environment for testing the influence of the torque feedback before implementing the torque emulation component into the real telestation. The main differences between the real telestation and the simulator are that in the simulator the vehicle is operated in a simulation environment, communication time delay is constant, and animation of the vehicle is only delayed by half of the RTT. In the Figure 3.3, the schematic structure of the teledriving simulator is illustrated. For simplicity, the pedal inputs are not shown.

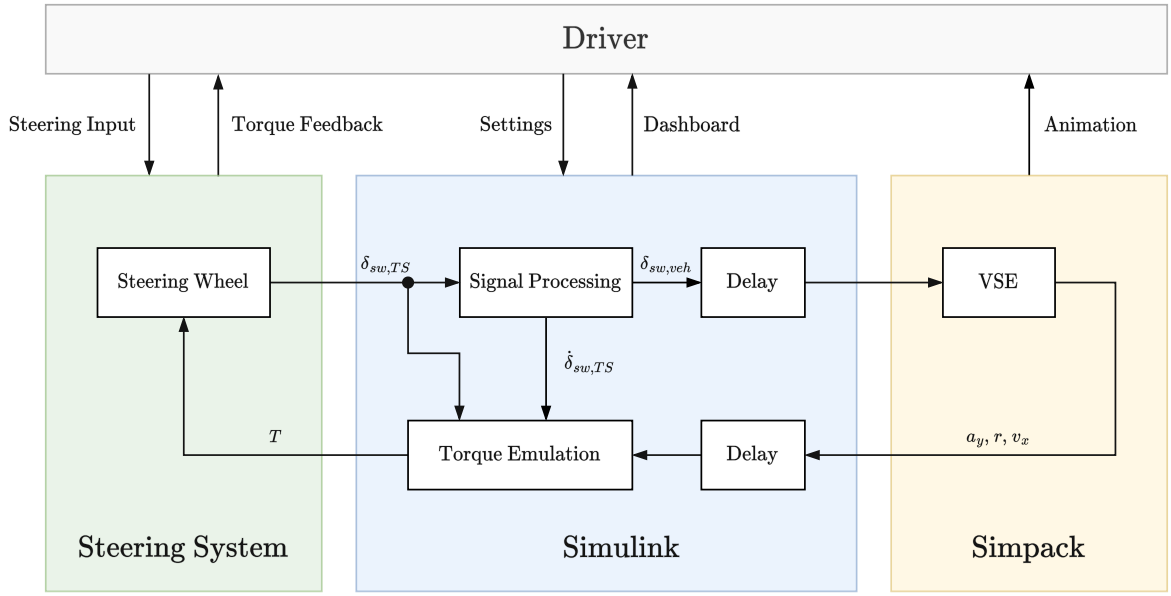

Figure 3.3.: Schematic diagram of the teledriving simulator

The steering system is the only hardware component in the simulator. It transmits the steering inputs and pedal positions to Simulink [26]. The steering wheel angle and pedal positions at the simulator steering system are processed and delayed in Simulink to match the real teleoperation system. Since the focus of this thesis is on torque emulation, the transmission of the pedal position is not further discussed. In Simulink, the steering wheel angle of the vehicle $\delta_{sw,veh}$ is evaluated and transmitted as the input to the vehicle simulation environment (VSE) in Simpack [27]. Virtual measurements of the vehicle's lateral acceleration, yaw rate, and longitudinal velocity from the VSE are delayed in Simulink and provided to the torque emulation component. In addition, the steering wheel angle and the calculated steering wheel angle rate are also transmitted to the torque emulation component. The torque emulation component evaluates the feedback torque T and sends it to the steering wheel. The driver feels the haptic feedback on the steering wheel and is provided with the animation of the vehicle from Simpack.

Furthermore, in Simulink, there is a dashboard where the driver can view the longitudinal velocity. The dashboard also allows the operator to change the torque emulation mode, select different tracks, and enable a speed controller for maintaining a constant longitudinal velocity.

3.1. Vehicle Simulation Environment (VSE)

As stated above, the VSE is implemented in Simpack (Figure 3.4). Simpack is used to build a sophisticated multi body model of the vehicle. It also provides the feature to build user defined roads with different maximum friction coefficients and unevenness. However, in the course of this thesis, only even roads are considered. In addition, measurements of any desired vehicle states and forces can be conducted easily. With the real time solver and animation option of Simpack, the simulation of the VSE can be executed and even animated in real-time.

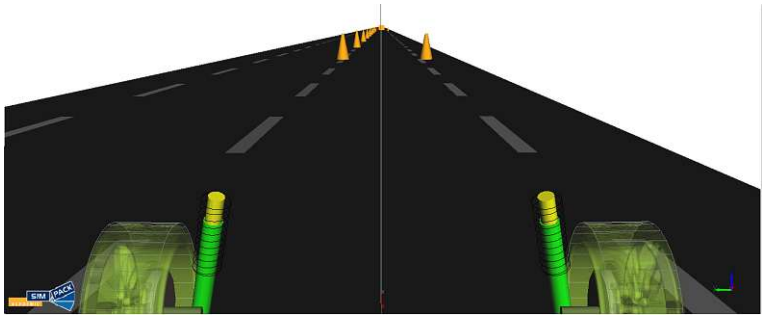

Figure 3.4.: Virtual Simulation Environment (VSE)

To fit the teleoperated vehicle of Vay, the wheelbase, mass, and the inertia of an existing Simpack vehicle of the Institute of Mechanics and Mechatronics are modified. As tyre model, the Pacejka tyre model in form of a TYDEX file is included and fitted to the vehicle of Vay. The vehicle's parameters are summarised in the Table 3.1 at the end of this chapter.

3.2. Steering System

The steering wheel of Thrustmaster model T300 is used, as the steering device. The throttle and brake pedals are not used since the driving task is done at a constant

velocity. The steering wheel is linked to the computer through an USB port. The steering wheel angle is measured and transmitted to Simulink. The range of the steering wheel angle can be adapted with a Thrustmaster control panel and is set to ±450 deg, like in the telestation of Vay. Furthermore, the steering system can receive torque reference values between ±1. The maximum generated torque is 3.9 Nm. It should be noted that a positive torque reference value leads to a clockwise torque, although the positive counting direction of the steering wheel angle is anticlockwise. The Figure 3.5 shows the steering wheel of Thrustmaster model T300.

Figure 3.5.: Thrustmaster T300

3.3. Signal Processing and Communication

The interface between the steering system and the VSE is Simulink. In Simulink, the steering wheel angle of the teledriving simulator is processed prior it is transmitted to Simpack. The steering wheel angle rate is calculated with the Backward-Euler scheme. The step time is set to 0.01 s and is denoted as ΔT.

$$\dot{\delta}_{sw,TS}(t) = \frac{\delta_{sw,TS}(t) - \delta_{sw,TS}(t - \Delta T)}{\Delta T} \tag{3.1}$$

To reduce noise, the steering angle rate is filtered and sent to the torque emulation component along with the steering wheel angle. Following that, the steering wheel angle is delayed by 0.04 s. Since the range of the steering wheel angle at the telestation $\delta_{sw,TS}$ is ±450 deg and the vehicle's steering wheel angle $\delta_{sw,veh}$ range is ±430 deg, the steering device ratio i_{sd} is introduced. To map the steering wheel angle at the telestation $\delta_{sw,TS}$ to the vehicle's steering wheel angle reference $\delta_{sw,veh,ref}$, the steering wheel angle at the telestation $\delta_{sw,TS}$ is divided by the steering device ratio i_{sd}. Additionally, the rate of

steering wheel input is limited to 300 deg/s to ensure safety in the case of software or hardware failure.

The steering task in the real vehicle is done by an internal controller. The identification of the internal controller behaviour is done with an ARX (autoregressive with exogenous input) model. The advantage of the ARX model is that it has a simple structure. The system transfer function and the noise filter have the same denominator. Furthermore, it allows efficient calculation and provides good results for low measurement noise. The structure of the ARX model is given in Figure 3.6. The deterministic input, also referred as to exogenous input, is $u(k)$. The stochastic input or the white noise is denoted as $v(k)$ and the output is $y(k)$ [28].

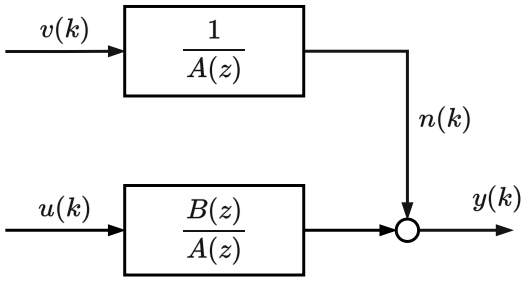

Figure 3.6.: Structure of the ARX model [28]

The identified transfer function of the internal controller is given below:

$$G_{C,int}(z) = \frac{B(z)}{A(z)} = \frac{\delta_{sw,veh}(z)}{\delta_{sw,veh,ref}(z)} = \frac{0.131z - 0.12}{z^3 - 2.077z^2 + 1.359z - 0.271} \tag{3.2}$$

Finally, the vehicle's steering wheel angle $\delta_{sw,veh}$ is divided by the steering ratio of the vehicle i_v and transmitted to the Simpack vehicle. In the following, the real telestation operating a real vehicle is compared with the teledriving simulator. Therefore, measurements of the real teleoperation system are used. To facilitate the comparison of both systems, the measured telestation steering wheel angle of the real teleoperation system is provided as steering input of the telestation simulator. Thus, only the measured steering wheel angle is depicted in the upper plot of the Figure 3.7. The lower plot of the Figure 3.7 shows the measured vehicle steering wheel angle and the vehicle steering wheel angle of the simulator. It can be seen that the simulator reproduces the same vehicle steering wheel angle $\delta_{sw,veh}$ as the measurements of the real teleoperated system.

This indicates that the teledriving simulator accurately replicates the signal processing, telecommunication network, and vehicle of the real teleoperation system.

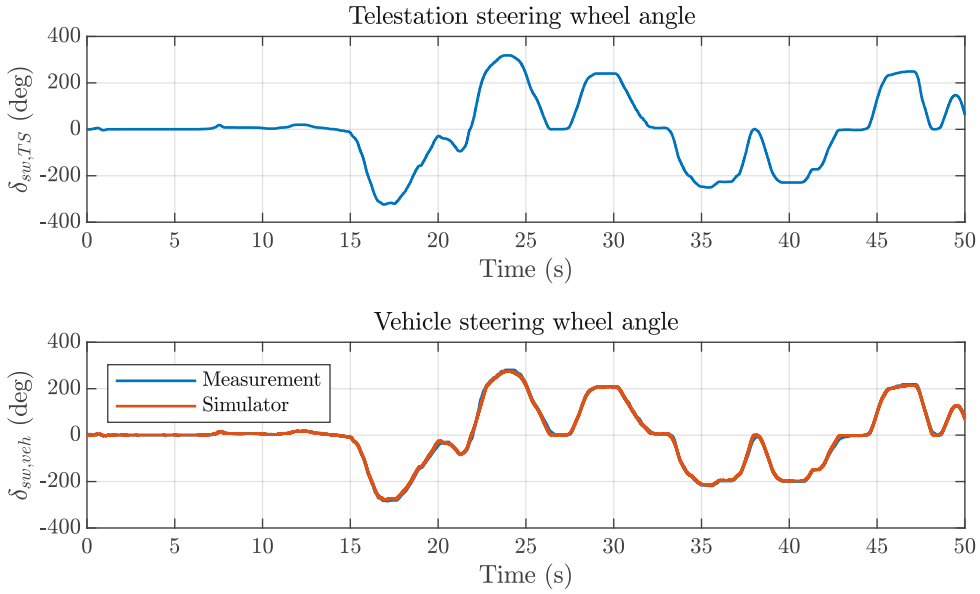

Figure 3.7.: Comparison of the vehicle steering wheel angle measurement of the real teleoperated system and the vehicle steering wheel angle of the simulator

The lateral acceleration and the yaw rate of the simulator are compared with the measurements of the real vehicle in Figures 3.8, and 3.9. It shows that the response of the simulated vehicle in Simpack and the real teleoperated vehicle match. The results demonstrate that the teledriving simulator can serve as a highly accurate test and training environment for the real teleoperation system.

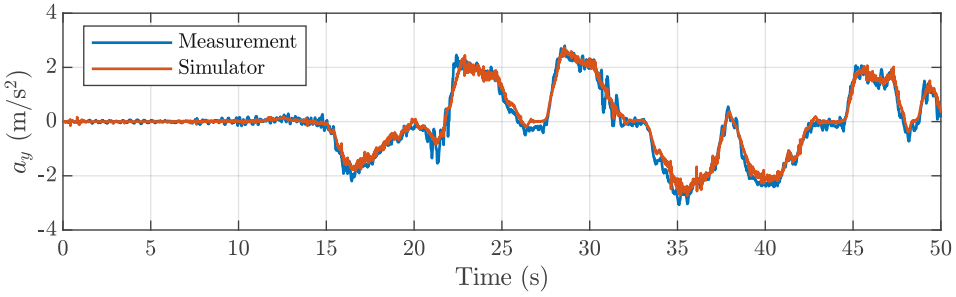

Figure 3.8.: Validation of the lateral acceleration

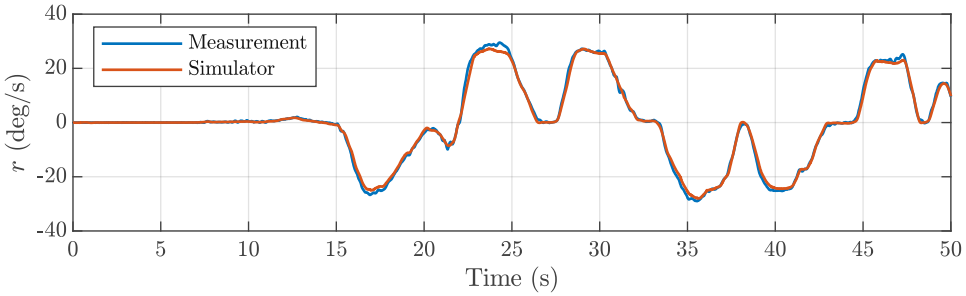

Figure 3.9.: Validation of the yaw rate

3.4. Linear Two-Wheel Vehicle Model

In the case of a very high communication time delay, receiving the telemetry signals may take a considerable amount of time. Likewise, in the case of a software failure, there might be no telemetry signals at all. To provide the teledriver with the information of the vehicle in such cases, the linear two-wheel vehicle model, also known as the bicycle model, is introduced. The main advantages are the simple structure of the model and that the response of the model is not affected by the communication time delay since the telestation steering wheel angle can be utilised to calculate the model input. The linearised equation of motion with constant longitudinal velocity v_x for the model shown in Figure 3.10, are given.

$$mv(\dot{\beta} + \dot{\psi}) = F_{yF} + F_{yR} \tag{3.3}$$

$$I_z\ddot{\psi} = F_{yF}l_F - F_{yR}l_R \tag{3.4}$$

The mass is m, the vehicle side slip angle rate is $\dot{\beta}$, the yaw rate is $\dot{\psi}$ or r, the lateral tire forces are F_{yi}, the moment of inertia with respect to the vertical axis at the centre of gravity is I_z and the semi-wheel bases are l_i $(i = F, R)$. The parameters of the two-wheel vehicle model are given in Table 3.1.

The front and rear $(i = F, R)$ lateral tyre forces are calculated with a linear approach using the cornering stiffness C_i and the linearised side slip angle α_i :

$$F_{yi} = C_i\alpha_i \tag{3.5}$$

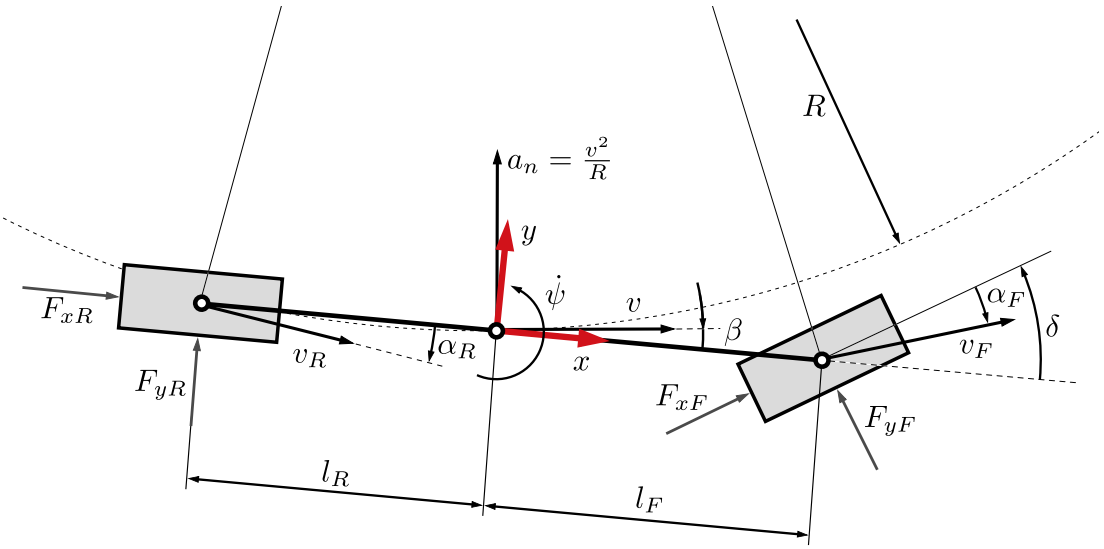

Figure 3.10.: Two-wheel vehicle model [21]

$$\alpha_F = \delta - \beta - \frac{\dot{\psi} l_F}{v_x} \tag{3.6}$$

$$\alpha_R = -\beta + \frac{\dot{\psi} l_R}{v_x} \tag{3.7}$$

The state space model can be derived with the equations (3.3)-(3.7) and has the following structure:

$$\dot{\underline{x}} = \boldsymbol{A}\underline{x} + \underline{b}u \tag{3.8}$$

$$\begin{bmatrix} \dot{\beta} \\ \dot{r} \end{bmatrix} = \begin{bmatrix} -\frac{C_F + C_R}{m v_x} & -\frac{l_F C_F - l_R C_R}{m v_x^2} + 1 \\ -\frac{l_F C_F - l_R C_R}{I_z} & -\frac{l_F^2 C_F + l_R^2 C_R}{I_z v_x} \end{bmatrix} \begin{bmatrix} \beta \\ r \end{bmatrix} + \begin{bmatrix} \frac{C_F}{m v_x} \\ \frac{l_F C_F}{I_z} \end{bmatrix} \delta \tag{3.9}$$

The transfer functions $G_r(s)$ and $G_\beta(s)$ are evaluated with the output matrix $\boldsymbol{C}$:

$$\boldsymbol{C} = \begin{bmatrix} 1 & 0 \\ 0 & 1 \end{bmatrix} \tag{3.10}$$

$$\begin{bmatrix} G_\beta(s) \\ G_r(s) \end{bmatrix} = \boldsymbol{C}(\boldsymbol{I}s - \boldsymbol{A})^{-1}\underline{b} \tag{3.11}$$

The input u can be changed from the road wheel angle δ to the telestation steering wheel angle $\delta_{sw,TS}$ with the total steering ratio i_L. The total steering ratio i_L is evaluated with the steering device ratio i_{sd} and the kinematic steering ratio i_v.

$$i_L = i_{sd} i_v \tag{3.12}$$

$$\delta = \frac{1}{i_L} \delta_{sw,TS} \tag{3.13}$$

The vehicle's lateral acceleration and the yaw rate of the linear bicycle model are compared with the Simpack vehicle in Figures 3.11 and 3.12. The figures demonstrate that the linear bicycle model's response closely matches the more sophisticated Simpack vehicle's response in the linear region (up to $4\,\mathrm{m/s^2}$). The response of the Simpack vehicle, representing the real vehicle, is delayed due to communication delay. Thus, the two-wheel vehicle model can be used as a backup model in case of any issue where the vehicle states are not transmitted properly or the communication time delay is too high.

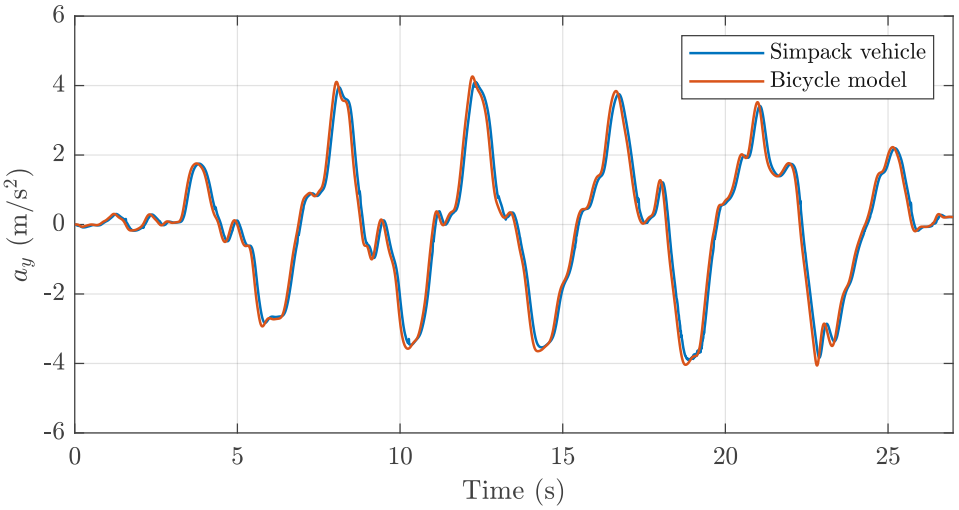

Figure 3.11.: Comparison of the lateral acceleration of the Simpack vehicle and the linear bicycle model

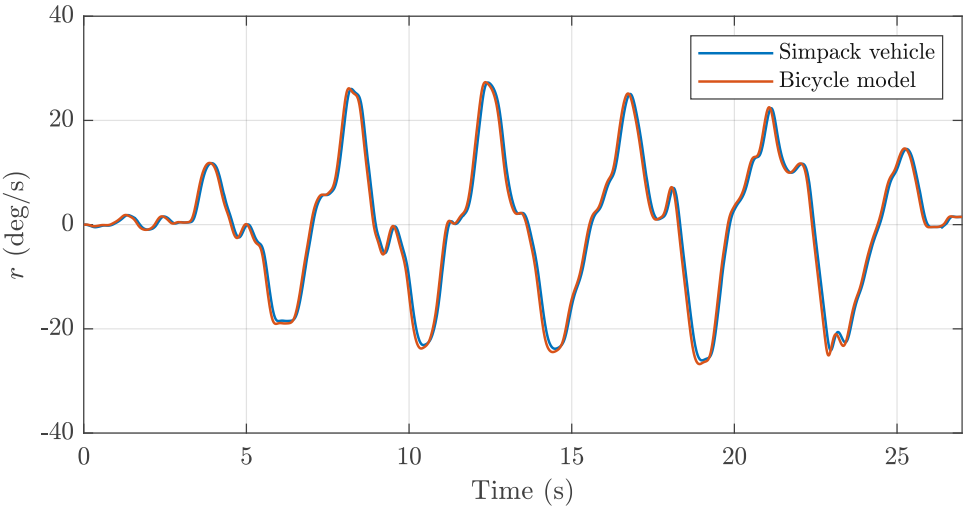

Figure 3.12.: Comparison of the yaw rate of the Simpack vehicle and the linear bicycle model

Parameter	*Value*	*Unit*	*Description*
l	2.72	m	Wheelbase
l_F	1.31	m	Front semi-wheelbase
l_R	1.41	m	Rear semi-wheelbase
m	1812	kg	Mass of the vehicle
I_z	2006	kgm^2	Inertia around vertical axis
C_F	121 400	N/rad	Front cornering stiffness
C_R	119 990	N/rad	Rear cornering stiffness
i_{sd}	1.071	1	Steering device ratio (from telestation to vehicle)
i_v	13.3	1	Kinematic steering ratio
i_L	14.25	1	Total steering ratio

Table 3.1.: Parameters of the two-wheel vehicle model

4. Torque Emulation

As described in Section 1.2, there are many concepts to emulate the feedback torque at the steering wheel. However, most of them require a profound knowledge of the steering system parameters. In the scope of this study, basic ideas from the literature are merged to develop a simple torque emulation method, that can be easily implemented in every teleoperated vehicle-teledriver system. This torque emulation method is not necessarily about providing the teledriver with the steering torque feedback of a real vehicle. The aim is to provide the teledriver with a steering feel, that improves perception and the maneuverability of the teleoperated vehicle. Since there are no physical links between the telestation steering system and the vehicle steering system the feedback torque can be generated freely.

In Figure 4.1 the structure of the torque emulation concept is illustrated. It has a modular structure that can be tuned as described in [17].

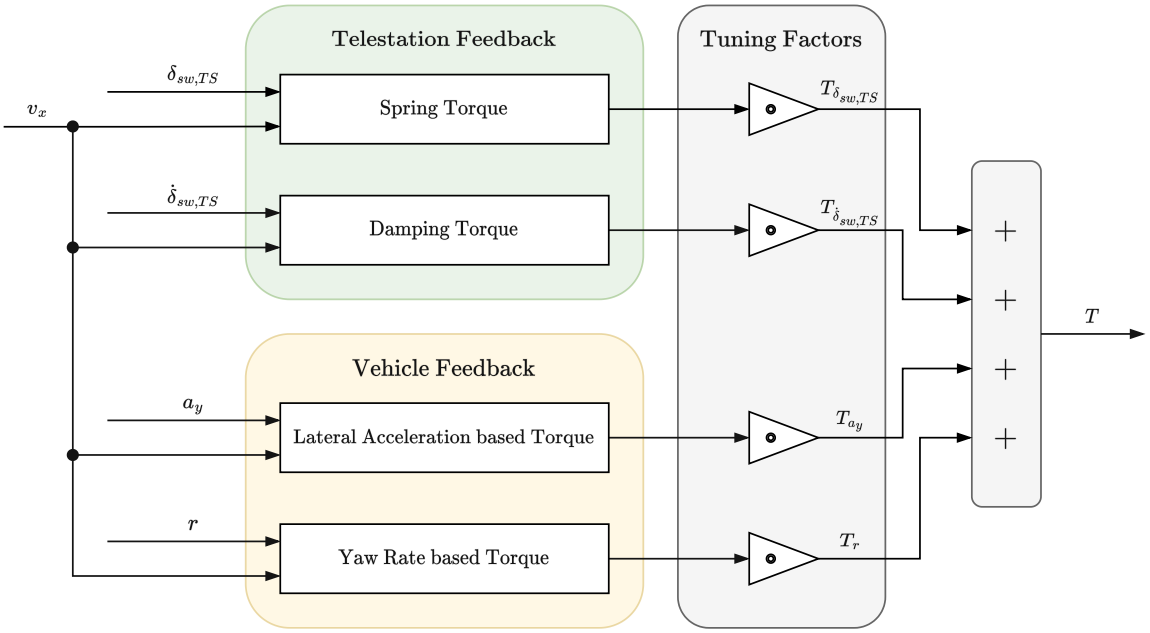

Figure 4.1.: Structure of torque emulation concept

The feedback torque can be categorised into two groups: Telestation feedback and vehicle feedback. The telestation feedback is dependent on the teledriver inputs at the

telestation, such as the steering wheel angle $\delta_{sw,TS}$ and the steering angle rate $\dot{\delta}_{sw,TS}$. Based on the steering wheel angle a spring torque and based on the steering angle rate a damping torque is calculated. The vehicle feedback is dependent on the lateral acceleration a_y and the yaw rate r. The lateral acceleration and the yaw rate based torques are used to provide the teledriver with the information of the vehicle. Each torque component T_i is evaluated with a two-dimensional characteristic curve that considers the longitudinal velocity v_x. The characteristic curves are generated with the hyperbolic tangent function. The maximum value and the slope around the origin are varied with the parameters $A_i(v)$ and $\xi_i(v)$. The variable and the index i describe the used signal to generate the torque component ($i = \delta_{sw,TS}$, $\dot{\delta}_{sw,TS}$, a_y, r).

$$T_i = A_i(v) \tanh(\xi_i(v) \cdot i) \tag{4.1}$$

The advantage of this approach is that the characteristic curves can be easily adapted. To understand how $\xi_i(v)$ influences the slope, the following expression can be used:

$$\xi_i(v) \approx \frac{2}{i_{96\%}} \tag{4.2}$$

Depending on the value $i_{96\%}$ at which 96 % of the maximum value of the torque $A_i(v)$ should be reached, $\xi_i(v)$ can be chosen [17]. In Figure 4.2 the influence of ξ_i on the characteristic curves is exemplified by the lateral acceleration based torque.

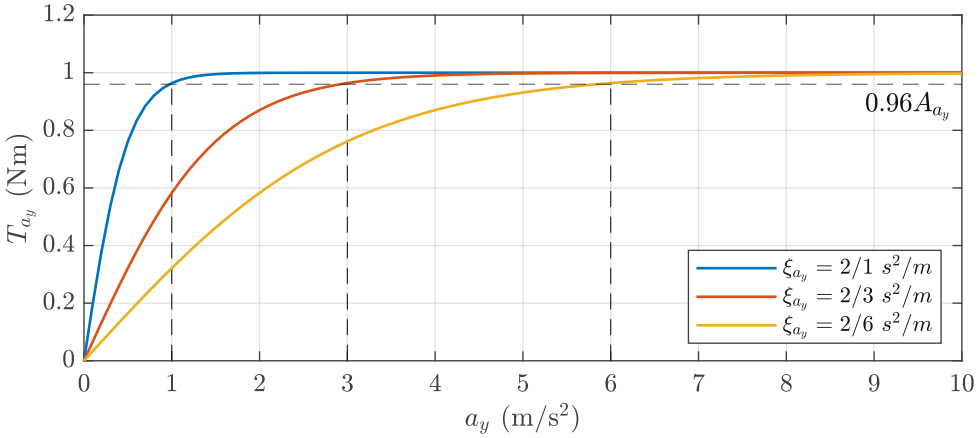

Figure 4.2.: Dependence of ξ_i on the characteristic curves [17]

Before summing up the torque components, the contribution of each torque component can be weighted by tuning factors. These tuning factors can also be used to create

different torque emulation modes that take into account some of the torque components or even create user defined steering feedback settings for different telestation operators. The latter is not further investigated in the scope of this study. If needed, the feedback torque T can be scaled depending on the maximum steering torque and how the steering system receives the steering torque reference values.

It should be noted, that the lateral acceleration, the yaw rate, and the longitudinal velocity are measured at the teleoperated vehicle and transmitted to telestation with a time delay. Thus, the response of the vehicle feedback is delayed, whereas the response of the telestation feedback is immediate. This might lead to an artificial steering feedback. In the case of any issue where the vehicle states are not transmitted properly or the communication time delay is too high, the states from the two-wheel vehicle model can be used.

In Table 4.1, the implemented torque emulation modes and the corresponding torque components are given. For each mode, there is a tuning factor set that can be adapted, if necessary. The torque emulation modes 1-4 are used for testing the contributions of each torque component. Torque emulation mode 0 represents no feedback at the steering wheel. In the following, the torque components are described in more detail. Therefore, the characteristic curves with the tuning factor set of the torque emulation mode 9 are shown, as it considers all torque components.

Torque emulation mode	*Torque components*
0	–
1	$T_{\delta_{sw,TS}}$
2	$T_{\dot{\delta}_{sw,TS}}$
3	T_{a_y}
4	T_r
5	$T_{\delta_{sw,TS}}$, $T_{\dot{\delta}_{sw,TS}}$
6	$T_{\dot{\delta}_{sw,TS}}$, T_{a_y}
7	$T_{\delta_{sw,TS}}$, $T_{\dot{\delta}_{sw,TS}}$, T_{a_y}
8	$T_{\delta_{sw,TS}}$, $T_{\dot{\delta}_{sw,TS}}$, T_r
9	$T_{\delta_{sw,TS}}$, $T_{\dot{\delta}_{sw,TS}}$, T_{a_y}, T_r

Table 4.1.: Torque emulation modes and the corresponding torque components

4.1. Spring Torque

The spring torque is dependent on the steering wheel angle of the telestation and the longitudinal velocity v_x. The behaviour is similar to a spring, as the name indicates. The torque rises with increasing steering angle in a degressive manner at a certain velocity. With increasing longitudinal velocity the maximum torque and the slope around the origin increases. The steering wheel gets stiffer with increasing velocity at the same steering angle. That provides the driver with a safer steering feel at higher velocity [17]. Additionally, the spring torque has a self-centring behaviour that brings the steering wheel back to the centre position. Since the steering wheel angle is measured at the telestation, an immediate response can be generated. The characteristic curves of the spring torque at different velocities are given in Figure 4.3.

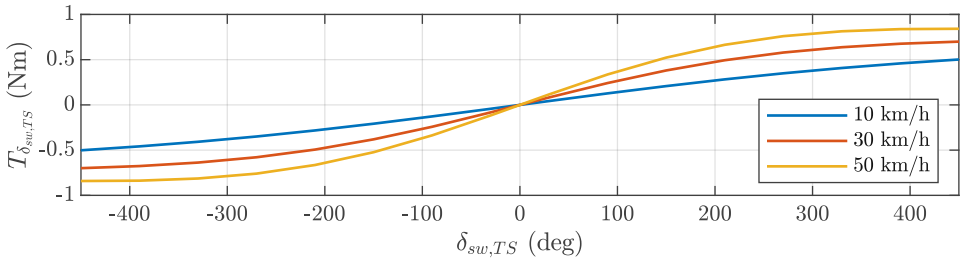

Figure 4.3.: Characteristic curves of the spring torque

4.2. Damping Torque

The damping torque depends on the steering angle rate that is calculated based on the steering wheel angle. It is an essential part as it prevents the driver from steering rapidly and gives the teledriver the feeling of steering a heavier car. The feeling of steering a heavier vehicle might lead to a better understanding of the delayed vehicle reaction at high velocities [5]. Additionally, this torque component damps the oscillations during self-centring and also reduces vibrations [17]. Like the spring torque, the damping torque increases with increasing steering angle rate. The slope around the origin and the maximum value of the damping torque increases with increasing longitudinal velocity, as shown in Figure 4.4. Furthermore, the a high damping torque can be used to reduce steering movements at standstill to reduce tyre wear out. In the scope of this study, this feature is not further investigated.

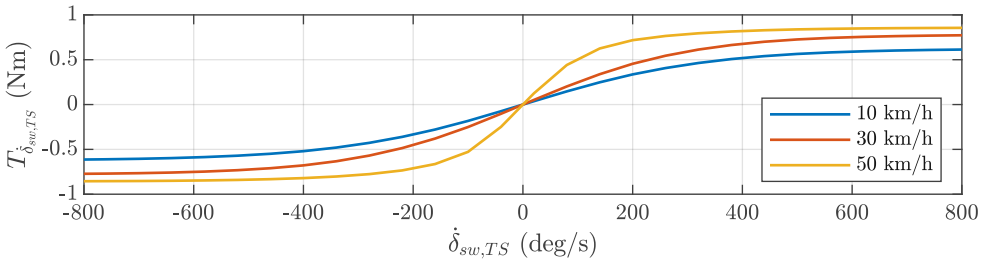

Figure 4.4.: Characteristic curves of the damping torque

4.3. Lateral Acceleration based Torque

The lateral acceleration based torque provides the teledriver with information of the vehicle's behaviour. As stated before, the transmission of the telemetry signal is delayed. If the delay is too large, the states of the two-wheel vehicle model can be used. That provides the teledriver with an immediate response. Nevertheless, it can be beneficial to use the measurement of the teleoperated vehicle. The torque component with the measured lateral acceleration can provide information of road unevenness to the driver. Rotations around the roll axis lead to a change in the measured lateral acceleration. The teledriver feels that in the form of small vibrations. Additionally, the delay might help the teledriver to understand that the vehicle response is delayed. The characteristic curves of the lateral acceleration based torque are given in Figure 4.5. The maximum value of the torque component increases with increasing longitudinal velocity. The gradient near the origin increases with decreasing velocity, ensuring that the teledriver continues to receive torque due to the vehicle information, as low velocities do not result in great lateral acceleration values. Similar to the spring torque, this torque tends to self-centre the steering wheel.

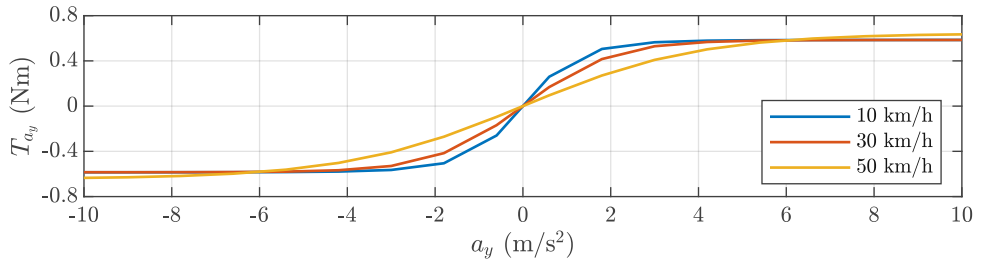

Figure 4.5.: Characteristic curves of the lateral acceleration based torque

4.4. Yaw Rate based Torque

The teledriver receives the information about the vehicle's angular rotation about the vertical axis in the form of yaw rate based torque. The yaw rate based torque's characteristics have similarities to the characteristic curves of the lateral acceleration based torque. The maximum value of the torque component increases with increasing velocity and the slope near the origin increases with decreasing velocity. As previously mentioned, the transmission of the telemetry signal is delayed. If this delay becomes significant, the yaw rate of the two-wheel vehicle model can be utilised for an instantaneous response. The yaw rate based torque has also the behaviour of self-centring of the steering wheel. The characteristic curves of the yaw rate based torque are illustrated in Figure 4.6.

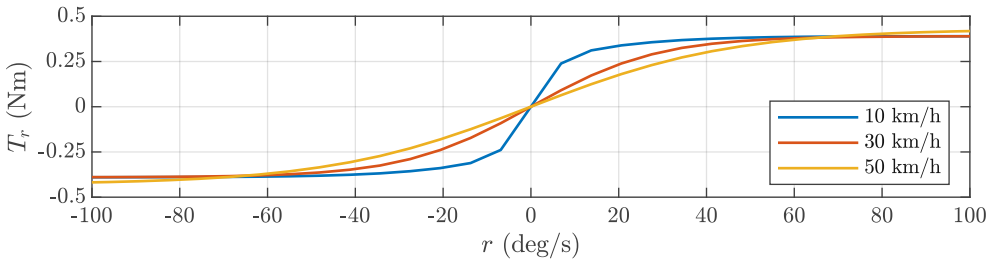

Figure 4.6.: Characteristic curves of the yaw rate based torque

5. Simulator Results

For testing the different torque emulation modes a slalom was built in Simpack. The distance between two cones is 18 metres and the width of the two lanes is 3 metres each. The gate of the slalom is placed 30 metres away from the starting point. Figure 5.1 shows the positions of the cones.

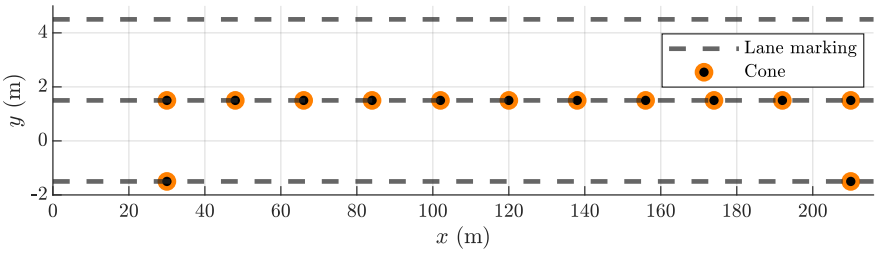

Figure 5.1.: Slalom

The task is to drive through the slalom at a constant velocity without hitting the cones and without leaving the lane borders. The vehicle's velocity is kept constant through the use of a speed controller and adjustments can be made within Simulink if required. In the Figure 5.2 the view of the slalom in Simpack is displayed.

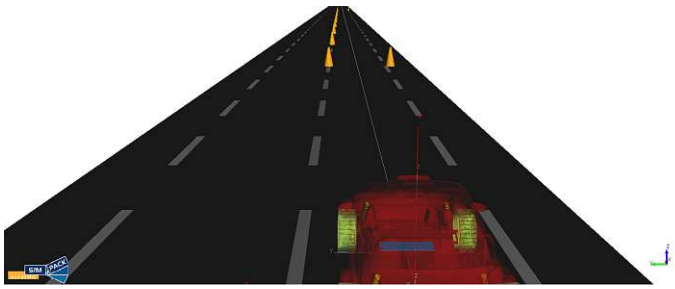

Figure 5.2.: Slalom in Simpack

The tests at the teledriving simulator have been performed by with multiple teledrivers with different experience levels. As examples, only two drivers with very different experience levels were chosen for the analysis. Driver 1 is a teledriver with little teledriving experience, while Driver 2 is a highly experienced teledriver. These results provide valuable insights into the specific driving behaviour of the drivers tested, but may not fully represent the broader range of teledriver driving behaviour.

5.1. Driving without Feedback Torque - Mode 0

5.1.1. Driving at 30 km/h

The first task of the teledrivers was to drive through the slalom without any feedback torque at $v_x = 30\,\text{km/h}$. In the Figure 5.3 the driven trajectories of the two drivers are shown. It clearly shows that Driver 1 has difficulties driving through the slalom without hitting the cones and without leaving the lanes. Whereas, Driver 2 drives through the slalom without touching any cones and stays on the road. Comparing the two drivers shows that Driver 1 has a higher lateral distance to the cones, also referred as the amplitude, than Driver 2. Passing the sixth cone Driver 1 comes off the track and does not manage to follow the specified slalom path. It is notable that the Driver 2 manages to keep an almost constant amplitude without any haptic feedback at the steering wheel.

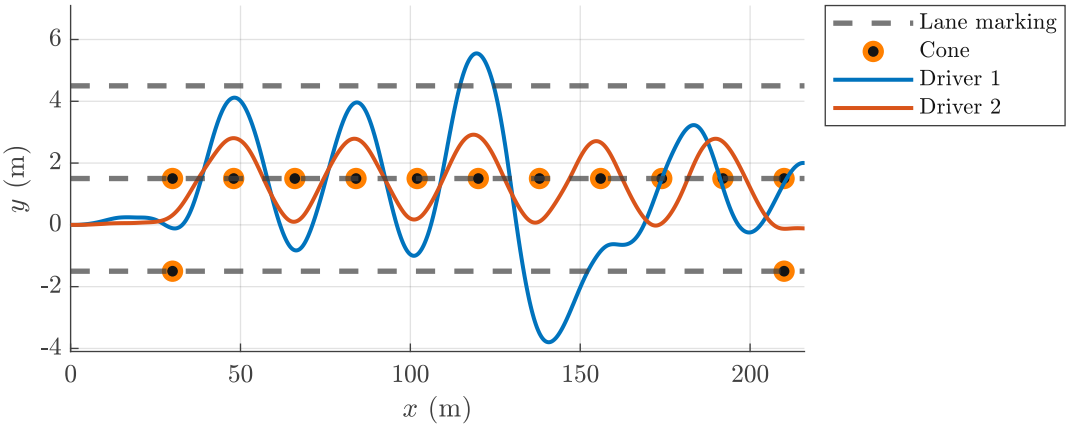

Figure 5.3.: Trajectory without feedback torque at $v_x = 30\,\text{km/h}$

Figure 5.4 illustrates the driver's inputs, including the steering wheel angle and steering wheel angle rate, along with the corresponding the vehicle's states such as lateral acceleration and yaw rate. It should be noted that the steering wheel angle rate is only calculated after the first second to avoid peak values during initialisation. These peaks would otherwise be utilised in the computation of the damping torque.

The steering wheel angle and the steering wheel angle rate of Driver 1 are higher than the steering wheel inputs of Driver 2 as expected. Driver 2 tends to steer slowly, which can be seen in the lower values for the steering wheel angle rate. Due to the slower

steering, Driver 2 seems less affected by the communication time delay, the rate limiter and vehicle steering system dynamics than Driver 1. The rate limiter is used for safety reasons in the real system and thus also in the simulator, particularly in cases of software failure that could result in a sudden, and rapid increase in the steering wheel angle. The rate limiter restricts the rate at which the steering wheel angle is transmitted to the vehicle, with a maximum rate of 300 deg/s. As the vehicle responds with a delay, Driver 1 tries to steer more and therefore has to compensate for the additional steering input by steering in the counter direction. This behaviour can be observed in the subplot illustrating the steering wheel angle rate, where Driver 1 steers rapidly after passing the slalom gate. As stated before, the transmission of the steering wheel signal has a rate limiter. That gives the driver the feeling of a huge delay when applying rapid steering wheel inputs, because of the slower vehicle response. Due to the higher steering wheel angle input of Driver 1, the corresponding lateral acceleration and yaw rate are also higher.

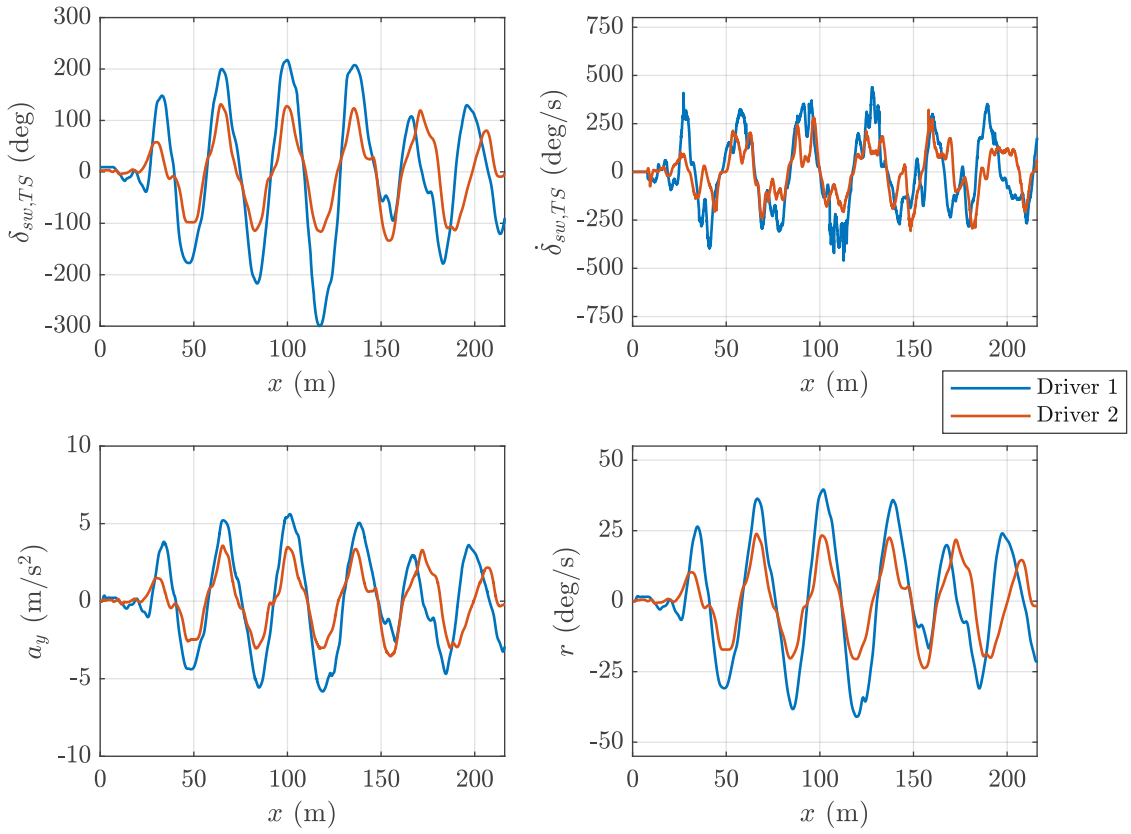

Figure 5.4.: Comparison of driver inputs and vehicle states without feedback torque at $v_x = 30\,\mathrm{km/h}$

5.1.2. Driving at 40 km/h

The same test has been performed at $v_x = 40\,\text{km/h}$. The trajectories of Driver 1 and Driver 2 are given in Figure 5.5. Again, Driver 1 fails to drive through the slalom in a stable manner without feedback torque at the steering wheel. At $v_x = 40\,\text{km/h}$, Driver 1 comes off the track after the fourth cone. Due to the high amplitude Driver 1 skips driving between cones 4 and 5, but manages to come back on the road and starts to drive through the slalom. The increase of the amplitude after passing each cone can be seen clearly. In comparison, Driver 2 drives through the slalom without touching any cones or coming off the track. Driver 2 also manages to keep the amplitude almost constant.

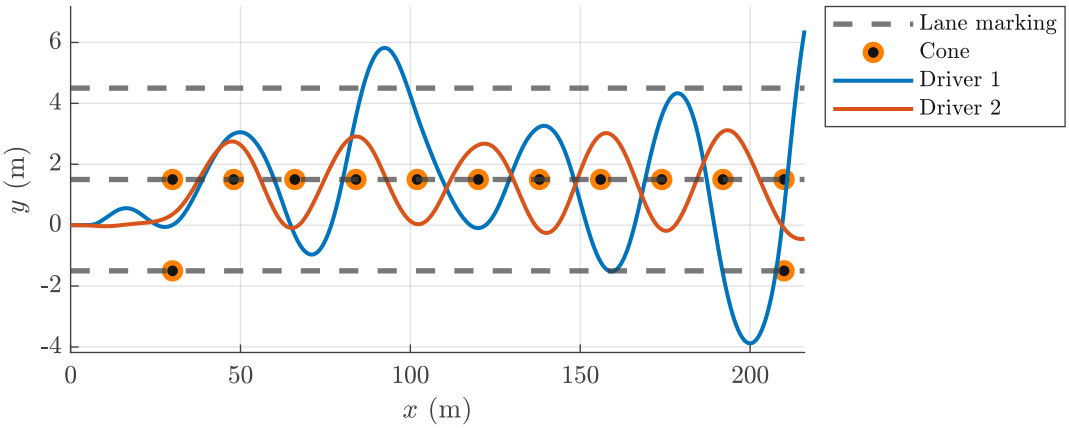

Figure 5.5.: Trajectory without feedback torque at $v_x = 40\,\text{km/h}$

The steering inputs of the drivers and the corresponding vehicle states are compared in Figure 5.6. The subplot, illustrating the steering wheel angle, shows that Driver 1 steers the vehicle to the left before passing the slalom gate and has to correct it with counter steering. The reason might be the lack of concentration. In general, the steering wheel angle of Driver 1 is larger and has more oscillations, indicative of correcting steering behaviour. On the other hand, the steering wheel angle input of Driver 2 is smaller and smooth. The steering wheel angle rate becomes very high before the vehicle motion with Driver 1 gets unstable. However, the maximum rate is limited causing the vehicle to react more slowly. Due to the slower reaction, Driver 1 steers more, ultimately resulting in a loss of control. In contrast, Driver 2 does not steer significantly more when the steering wheel angle rate is higher than the rate limit. Because of the large steering input of Driver 1, both lateral acceleration and yaw rate are notably high. The unstable

behaviour becomes also evident through the increasing lateral acceleration and the yaw rate.

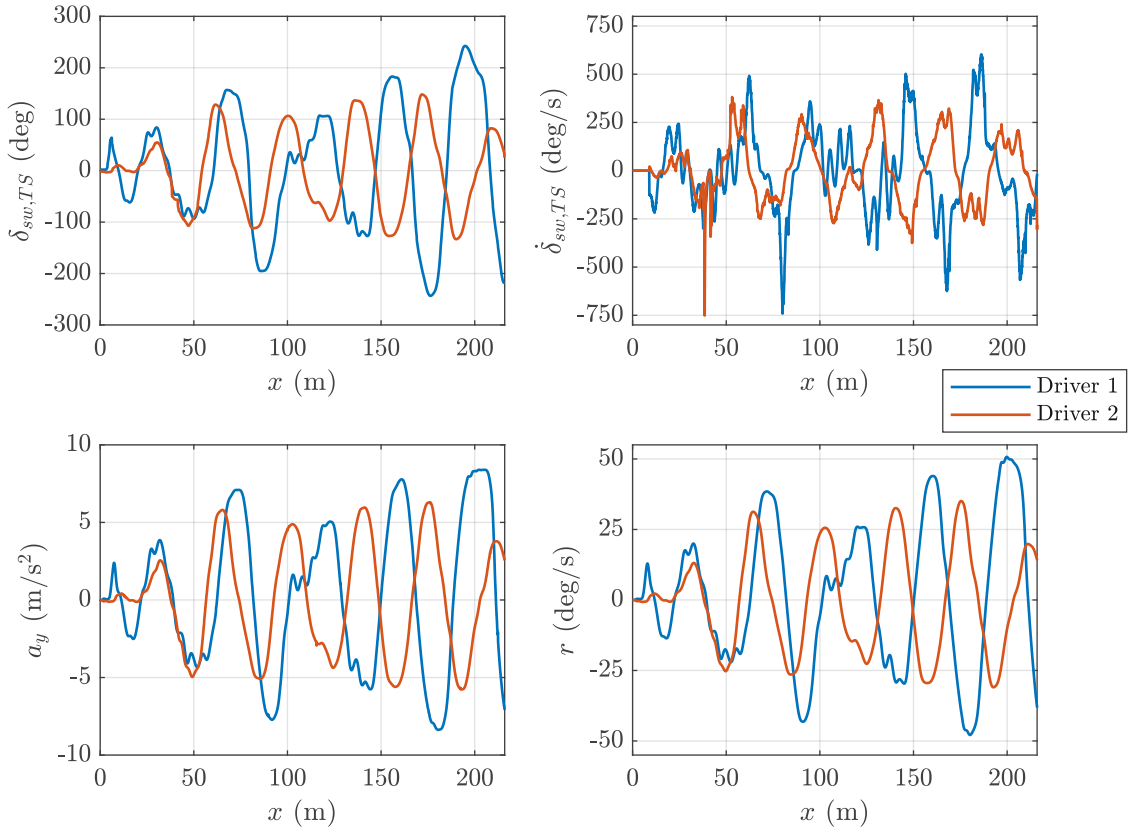

Figure 5.6.: Comparison of driver inputs and vehicle states without feedback torque at $v_x = 40\,\mathrm{km/h}$

The plots demonstrate that driving through the slalom without steering wheel feedback torque is possible at both $v_x = 30\,\mathrm{km/h}$ and $v_x = 40\,\mathrm{km/h}$ if the driver is a highly experienced teledriver. For new teledrivers or little experienced teledrivers like Driver 1, it is a difficult task to drive through the slalom without any torque feedback at the steering wheel. The Figures 5.4 and 5.6 indicate, that the less experienced teledriver tends to steer rapidly and does not consider the delayed vehicle response due to the missing perception of the vehicle.

5.2. Influence of the Torque Emulation

In this section, the reaction of Driver 1 to different torque emulation modes at different velocities is investigated. For a better overview, only modes 5 and 9 are compared with mode 0. Mode 5 only contains the spring and damping torque. Whereas, mode 9 considers all torque components. As shown in the past chapter, Driver 2 manages to steer the vehicle in a stable fashion without torque feedback. Therefore, the figures illustrating the steering behaviour of Driver 2 with torque feedback are given in the Appendix A.4.

5.2.1. Driving at 30 km/h

In Figure 5.7 the trajectories with the different torque emulation modes at $v_x = 30\,\mathrm{km/h}$ are illustrated. In comparison to mode 0, where no feedback torque is applied, Driver 1 successfully navigates through the slalom with the assistance of feedback torque. Moreover, the amplitudes are reduced with a feedback torque at the steering wheel. However, in mode 5, Driver 1 leaves the track after passing the exit gate of the slalom. In contrast, in mode 9, Driver 1 finishes the slalom without touching any cones, and not coming off the track. Additionally, Driver 1 manages to steer the vehicle with a slightly smaller amplitude than in mode 5.

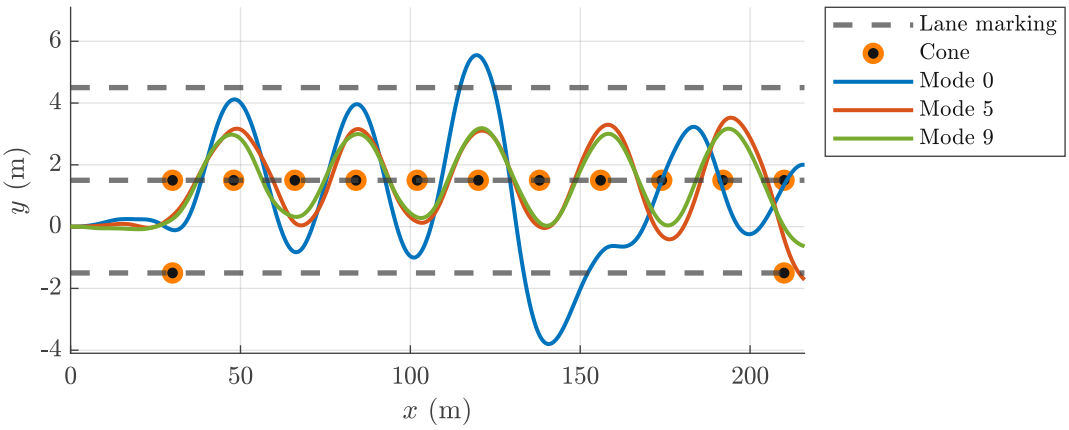

Figure 5.7.: Trajectory with different torque emulation modes at $v_x = 30\,\mathrm{km/h}$

The steering inputs of Driver 1 and the corresponding vehicle states with different torque emulation modes are compared in Figure 5.8. With feedback torque at the steering wheel,

the driver steers less than without feedback torque. Furthermore, in mode 9, Driver 1 reacts earlier passing the cones than in mode 5 or mode 0. Additionally, the steering wheel angle rate is lower in torque emulation mode 5 and 9 than with mode 0. Due to the lower steering wheel angle input in modes 5 and 9, the lateral acceleration and the yaw rate are also lower.

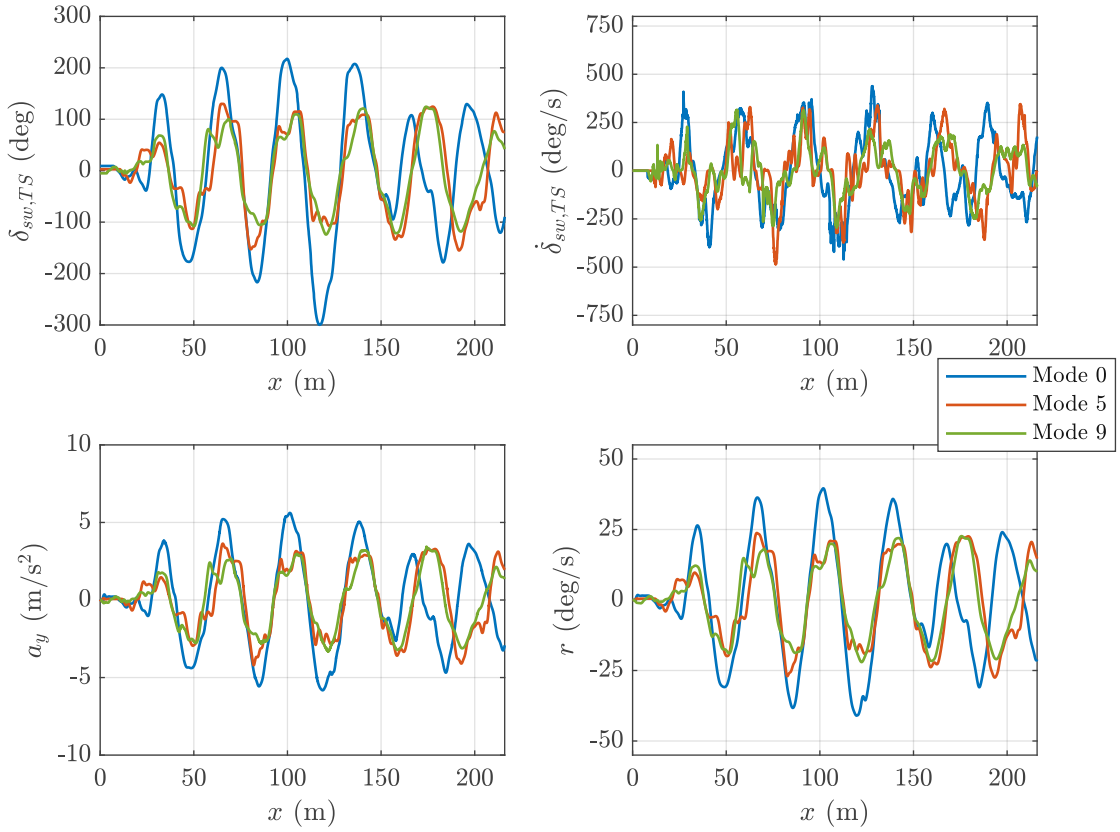

Figure 5.8.: Comparison of the steering inputs and vehicle states of Driver 1 with different torque emulation modes at $v_x = 30\,\mathrm{km/h}$

The feedback torque and the corresponding torque components for modes 0, 5 and 9 are plotted in Figure 5.9. The tuning parameters of mode 5 are chosen such that the spring torque has the greatest contribution. With increasing steering wheel angle, torque feedback increases. That steering wheel angle based torque may give the driver the feeling of having an immediate response, but the information of the vehicle's response is not provided. The feedback torque both in mode 5 and mode 9 have a maximum value around 1 Nm. In mode 9, the contribution of the spring torque is smaller, but there are additional torque components such as the lateral acceleration and the yaw

rate based torque. After the driver changes the steering wheel angle, the signal has to be transmitted to the vehicle and additionally, the lateral acceleration and the yaw rate have to build up. Due to the steering system dynamics of the vehicle, the lateral acceleration and yaw rate based torques do not fluctuate due to small movements at the steering wheel. That can be observed around $x = 120\,\text{m}$. A reason for the fluctuation of the feedback torque is the damping torque, which is dependent on the steering wheel angle rate. When driving at $v_x = 30\,\text{km/h}$ in mode 5, the steering wheel angle rate oscillates more, leading to oscillation in the resulting feedback torque.

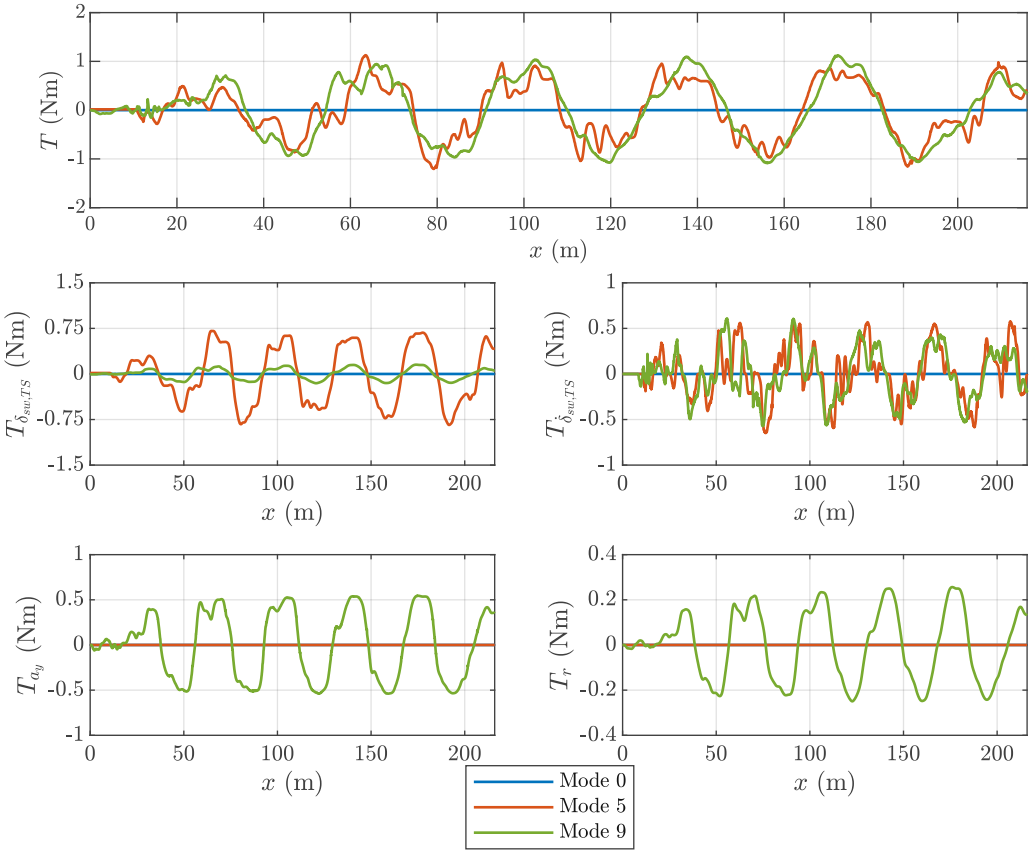

Figure 5.9.: Comparison of the torque components with different torque emulation modes at $v_x = 30\,\text{km/h}$ (Driver 1)

5.2.2. Driving at 40 km/h

Driving at $v_x = 40\,\text{km/h}$ with and without feedback torque, Driver 1 fails to finish the task without going off the track. However, with the presence of the feedback torque,

Driver 1 manages to progress further without leaving the track. With mode 5, Driver 1 manages to stay on the track until passing the tenth cone. With mode 9, Driver 1 only fails to drive through the exit gate of the slalom. In comparison, Driver 1 comes off the track after the fourth cone without the assistance of toque feedback. Figure 5.10 clearly shows the increase of the amplitude passing the cones, but with the haptic feedback, the amplitudes do rise slower than without haptic feedback. Moreover, the amplitudes are smaller with mode 9 than with mode 5 except of passing the fourth cone. There is a lateral movement of the vehicle before reaching the entrance gate when driving in mode 9. That can be explained by a non-centred steering wheel at the beginning of the test run. The lateral movement, when driving without torque feedback, may be due to lack of concentration as stated before. In both cases, Driver 1 manages to correct the lateral deviation before entering the slalom.

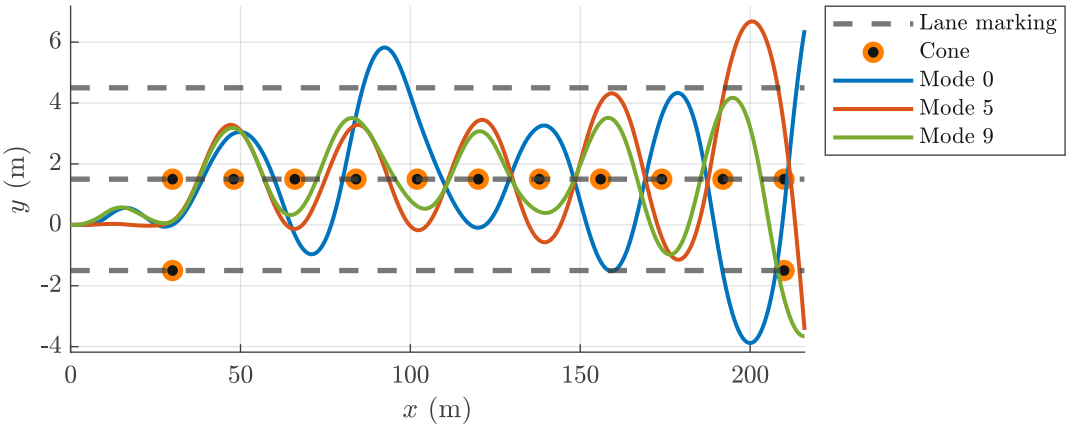

Figure 5.10.: Trajectory with different torque emulation modes at $v_x = 40\,\mathrm{km/h}$

Figure 5.11 shows the steering wheel angle, the steering wheel angle rate, lateral acceleration, and the yaw rate. The increase of the amplitude can be observed in the increasing steering wheel angle. It is notable that the steering wheel angle in mode 9 is applied earlier than at mode 5. Due to the heavy steering of Driver 1 at the end of the slalom, the lateral acceleration goes up to $8\,\mathrm{m/s^2}$ and the yaw rate reaches $50\,\mathrm{deg/s}$ in mode 9. Additionally, the steering wheel angle rate surpasses the rate limit. That might be the reason for the increasing steering wheel angle at the end of the slalom. With torque feedback, Driver 1 has fewer oscillations in the steering wheel angle, and the steering wheel angle rate than without torque feedback.

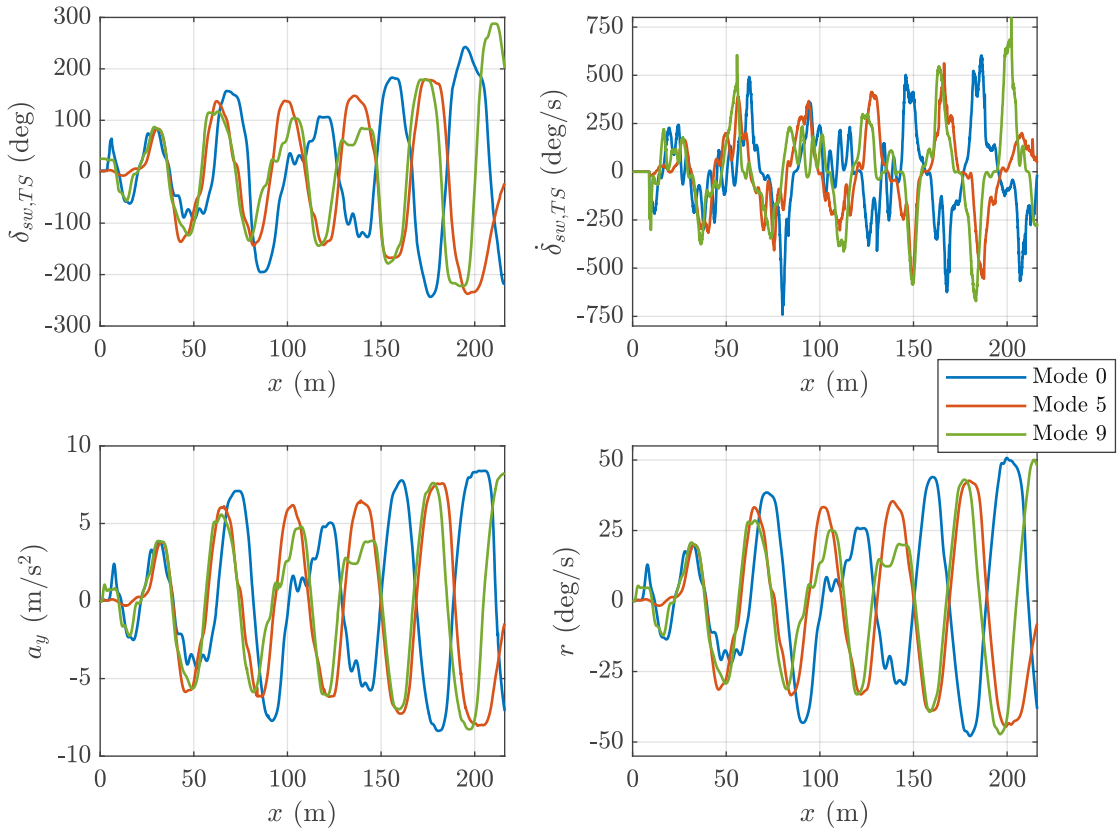

Figure 5.11.: Comparison of the steering inputs and vehicle states of Driver 1 with different torque emulation modes at $v_x = 40\,\mathrm{km/h}$

The torque components and the resulting feedback torque are plotted in Figure 5.12. In comparison to driving at $v_x = 30\,\mathrm{km/h}$, the feedback torque has a greater slope. Additionally, the magnitude of the maximum torque applied is higher. In general, torque components of the telestation feedback are higher at $v_x = 40\,\mathrm{km/h}$. The torque components of the vehicle feedback have a higher maximum values and provide more torque as higher lateral acceleration and yaw rates are reached with increasing speed. Before reaching the entrance gate of the slalom, the driver feels a feedback torque driving in mode 9. This is due to the off-centre steering wheel position at the beginning of the test run. After $x = 150\,\mathrm{m}$ the feedback torque in mode 5 consists more or less of the spring torque due to the high steering wheel angle. In mode 9, the feedback torque is provided with a small delay due to the communication over the internet and also because the vehicle's lateral acceleration and the yaw rate have to build up after a steering wheel input.

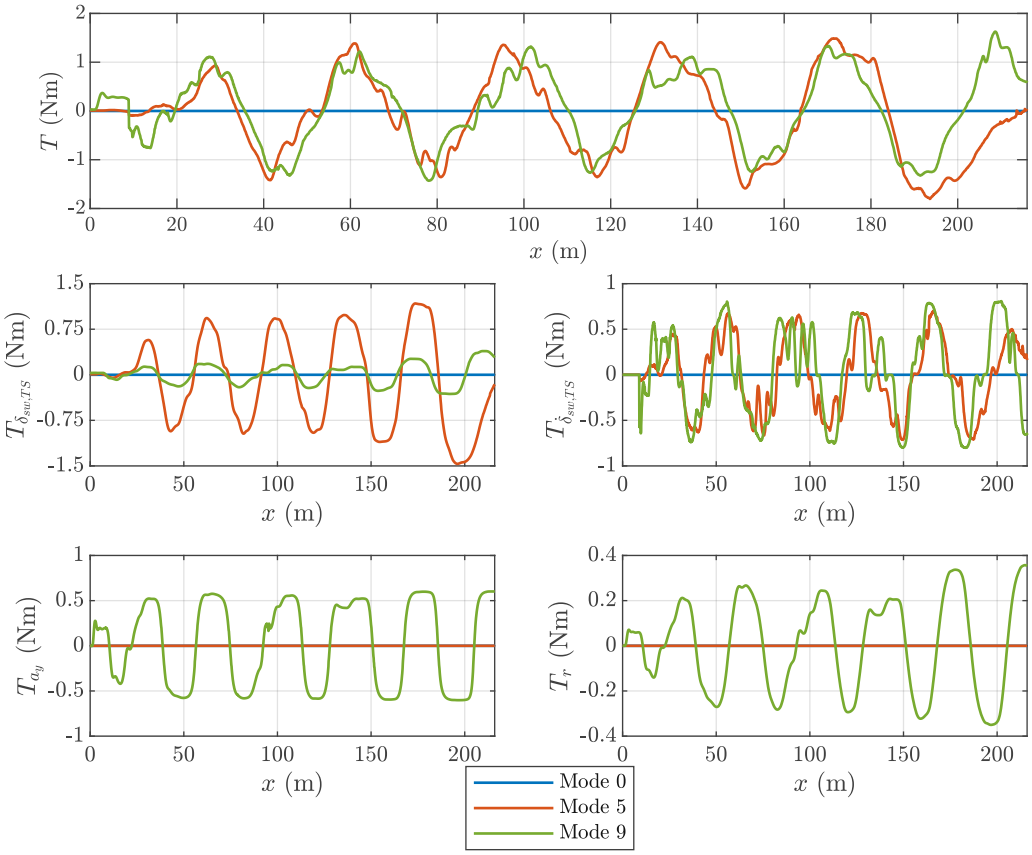

Figure 5.12.: Comparison of the torque components with different torque emulation modes at $v_x = 40\,\mathrm{km/h}$ (Driver 1)

6. Real Teleoperation System Resuls

After the testing at the teledriving simulator, the torque emulation component was integrated into the real telestation. The influence of the torque emulation modes was tested at the proving ground by different teledrivers. The testing ground has a parkour that includes a part of the slalom. The slalom at the testing ground is shorter and therefore not fully comparable to the slalom in the simulator. The slalom has four cones that have to be passed, and there is no entrance gate. In addition, there is no speed controller, which keeps the velocity at a constant value. In Figure 6.1, the driven trajectory by Driver 2 in mode 5 and mode 9 are illustrated as examples. The trajectories are measured with a GPS device. Thus, there is a slight measurement inaccuracy that can be observed. The amplitudes in both modes do not deviate much from each other.

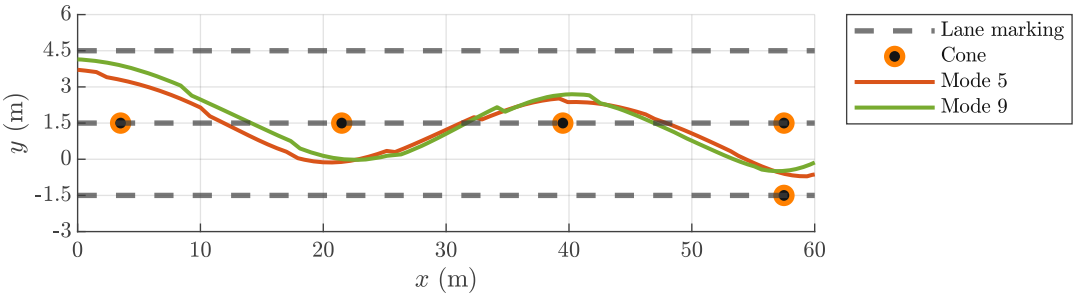

Figure 6.1.: Trajectories with different Torque modes at the testing ground

The steering wheel angle, steering wheel angle rate and the vehicle's states are shown in Figure 6.2. In mode 9, the driver drives with a higher velocity than in mode 5. Thus, the maximum values of the lateral acceleration, and the yaw rate are higher in mode 9. The steering wheel angle and the steering wheel angle rate in both modes are almost the same. The high steering wheel angle at the end of the slalom is due to a left turn after the exit gate. Around $x = 10\,\mathrm{m}$, small spikes can be observed in the lateral acceleration. That could result from uneven road surfaces causing the vehicle to roll and induce oscillations in the lateral acceleration.

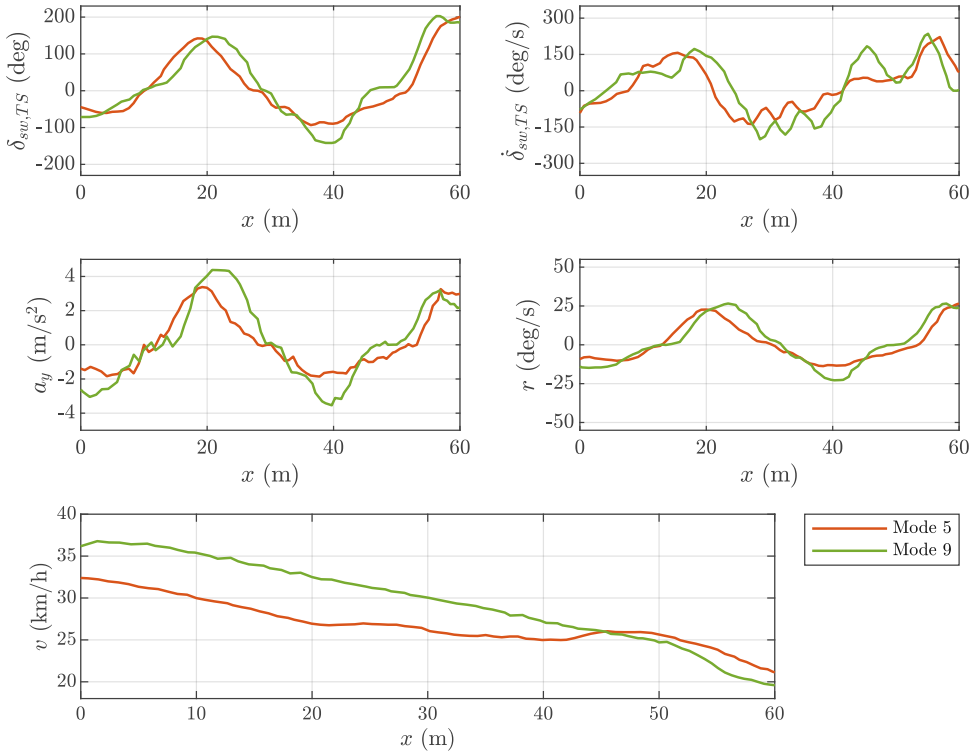

Figure 6.2.: Comparison of the steering inputs and vehicle states in different torque emulation modes at the testing ground

When comparing the feedback torque between the real teleoperation system (Figure 6.3) and the simulator, both systems provide nearly identical feedback while driving through the slalom. The significant difference in feedback torque between the telestation and the simulator lies in the sensation of road unevenness at the telestation in the form of small vibrations. This is due to the coupling of lateral and roll motion. However, this effect is absent in the simulator, as only even roads are considered.

Generally, the absence of feedback torque gives drivers an unusual light feeling. With torque feedback, particularly with the torque components of the vehicle feedback, the vehicle feels more responsive. Especially, the sensation of road unevenness, in the form of small changes in the feedback torque, is seen as valuable subjective information. Some teledrivers would prefer more damping torque, while others would prefer less. This could be achieved through individualised tuning parameter sets. Through tests being conducted on both the teledriving simulator and the actual telestation, it was demonstrated that torque feedback enhances teledriver perception of the teleoperated

vehicle and steering behaviour.

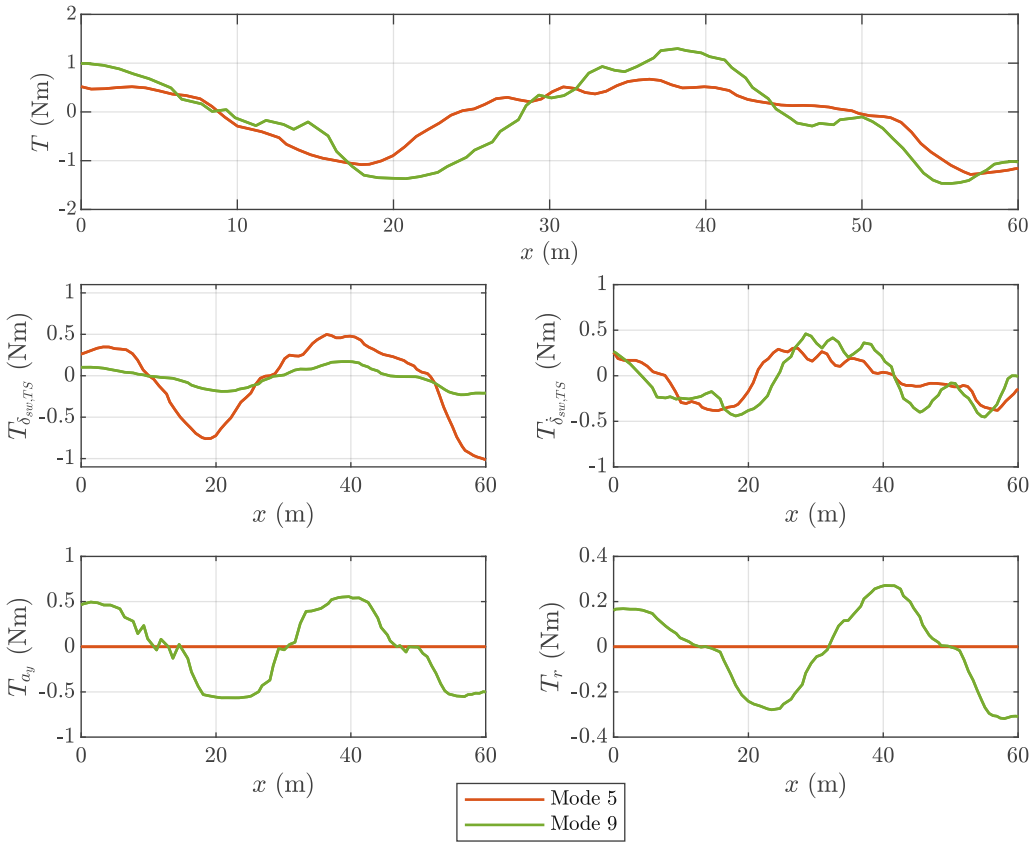

Figure 6.3.: Comparison of the torque components with different torque emulation modes at the testing ground

7. Conclusion and Outlook

Conclusion

This study shows from a theoretical perspective how the teleoperation of a vehicle differs from driving a normal vehicle. First of all, the influence of the communication time delay is shown. Even if the driver is able to adapt himself to changing driving conditions, the teleoperated vehicle-driver system may get unstable above a certain communication time delay. The missing perception of the vehicle is identified as another factor which might lead to an unstable system. In general, the teledriver has to cope with the influences of the time delay, which varies over time, and the missing perception. The combination of these two impacts makes the teleoperation of a vehicle a challenging task.

A teledriving simulator for testing the driving behaviour in a safe environment is developed successfully. It is demonstrated that reproducing the behaviour of the real teleoperation system of Vay, including its communication time delay and internal controllers, is feasible with the teledriving simulator.

To increase the driver's perception and the manoeuvrability of a vehicle, a simple structured, and tunable torque emulation concept is introduced, that considers the steering wheel angle, steering wheel rate, lateral acceleration, and the yaw rate. Due to the simple structure, it is possible to run the torque emulation component in real-time at the simulator and the real telestation.

The tests at the teledriving simulator demonstrate that a driver with little teledriving experience has difficulties driving without any torque feedback. Generally, the absence of feedback torque gives drivers an unusual light feeling. That leads to heavy steering due to the missing perception. It could be demonstrated that the system gets unstable whenever big steering wheel angle inputs are applied in combination with a high steering wheel angle rate. In this case, the driver tries to steer more due to the delayed reaction of the vehicle. The delayed reaction results from the communication time delay, rate limiter, and vehicle steering system dynamics. The integrated rate limiter restricts the maximum rate of the transmitted steering wheel angle to 300 deg/s. This feature is used

for safety reasons in the system, particularly in cases of software failure that could result in a sudden and rapid increase in the steering wheel angle. However, a higher maximum rate of the transmitted steering wheel angle might be considered to avoid delayed vehicle reaction due to the rate limiter. The less experienced teledriver is more affected by the delayed system than the experienced teledriver. The experienced teledriver manages to steer the vehicle with a lower steering angle and steering angle rate than the less experienced driver and thus finishes the slalom in a stable manner also without feedback torque.

With the assistance of torque feedback, the less experienced driver is able to finish the slalom without getting off the track at $v_x = 30\,\mathrm{km/h}$. At $v_x = 40\,\mathrm{km/h}$, this driver manages to travel further in a stable fashion than without any feedback torque. With the feedback torque, which includes both telestation feedback and vehicle feedback, the driver is able to drive with a smaller lateral deviation from the cones. Additionally, the driver steers less and at a lower steering angle rate. It should be noted that, only the results of two drivers with very different experience levels are shown in this analysis. These results provide valuable insights into the specific driving behaviour of the drivers tested, but may not fully represent the broader range of teledriver driving behaviour.

The conducted tests at the real telestation show similar results compared to the simulator. The haptic feedback provides the teledriver with a response from the vehicle and therefore helps with the steering task. Especially, the sensation of road unevenness, in the form of small vibrations is seen as valuable information. In summary, the tests conducted on both simulator and real telestation demonstrate that torque feedback holds significant potential in improving teledriver perception and steering behaviour.

Outlook

In the scope of this study, the behaviour of the teleoperated vehicle-teledriver system is investigated. It shows that it is necessary to have a component in the system that boosts the phase of the open loop system and therefore ensures the stability of the closed loop system. In the next step, the torque emulation component could be integrated into the teleoperated vehicle-teledriver system model to investigate its influence on stability.

Looking forward, there are possibilities for further investigation of the driving behaviour. One approach could involve constructing the complete slalom at the testing ground for a

more comprehensive investigation. Additionally, it is possible to integrate various other tracks into the simulator, expanding the scope of research. To enhance the overall understanding of torque feedback's influence on teledriver performance more test participants should be involved.

Bibliography

[1] On-Road Automated Driving (ORAD) committee, *Taxonomy and Definitions for Terms Related to Driving Automation Systems for On-Road Motor Vehicles*, Apr. 2021. [Online]. Available: https://www.sae.org/standards/content/j3016_202104/.

[2] N. Goodall, "Non-technological challenges for the remote operation of automated vehicles," en, *Transportation Research Part A: Policy and Practice*, vol. 142, pp. 14–26, Dec. 2020. DOI: 10.1016/j.tra.2020.09.024.

[3] T. Hoffmann and G. Prause, "On the Legal and Economic Implications of Tele-Driving," en, *Machines*, vol. 11, no. 3, p. 331, Mar. 2023. [Online]. Available: www.mdpi.com/2075-1702/11/3/331 (visited on 07/16/2023).

[4] A. Hosseini and M. Lienkamp, "Enhancing telepresence during the teleoperation of road vehicles using HMD-based mixed reality," in *2016 IEEE Intelligent Vehicles Symposium (IV)*, Jun. 2016, pp. 1366–1373. DOI: 10.1109/IVS.2016.7535568.

[5] C. Su, H. Li, and X. Wu, "Artificial Steering Feel for Teleoperated Road Vehicle with Disturbance Observer," in *2021 5th CAA International Conference on Vehicular Control and Intelligence (CVCI)*, Oct. 2021, pp. 1–6. DOI: 10.1109/CVCI54083.2021.9661125.

[6] A. Bhardwaj, D. Slavin, J. Walsh, J. Freudenberg, and R. B. Gillespie, "Estimation and decomposition of rack force for driving on uneven roads," en, *Control Engineering Practice*, vol. 114, p. 104 876, Sep. 2021. DOI: 10.1016/j.conengprac.2021.104876.

[7] T. Koch, "Untersuchungen zum Lenkgefühl von Steer-by-Wire Lenksystemen," Ph.D. dissertation, Technische Universität München, 2010. [Online]. Available: https://mediatum.ub.tum.de/977732.

[8] A. Marouf, M. Djemai, C. Sentouh, and P. Pudlo, "A New Control Strategy of an Electric-Power-Assisted Steering System," *IEEE Transactions on Vehicular Technology*, vol. 61, no. 8, pp. 3574–3589, Oct. 2012, Conference Name: IEEE Transactions on Vehicular Technology. DOI: 10.1109/TVT.2012.2209689.

[9] H. Zhang, Y. Zhang, J. Liu, J. Ren, and Y. Gao, "Modeling and characteristic curves of electric power steering system," in *2009 International Conference on Power Electronics and Drive Systems (PEDS)*, Nov. 2009, pp. 1390–1393. DOI: 10.1109/PEDS.2009.5385774.

[10] X. Jingyi, Z. Tao, L. Junjie, Z. Yang, G. Pingshu, and Y. Jingjing, "Research on EPS Assist Characteristics Based on Hardware-in-loop Simulation," in *2020 4th CAA International Conference on Vehicular Control and Intelligence (CVCI)*, Dec. 2020, pp. 525–529. DOI: 10.1109/CVCI51460.2020.9338654.

[11] J.-H. Kim and J.-B. Song, "Control logic for an electric power steering system using assist motor," en, *Mechatronics*, vol. 12, no. 3, pp. 447–459, Apr. 2002. DOI: 10.1016/S0957-4158(01)00004-6.

[12] D. Lee, K. Yi, S. Chang, B. Lee, and B. Jang, "Robust steering-assist torque control of electric-power-assisted-steering systems for target steering wheel torque tracking," en, *Mechatronics*, vol. 49, pp. 157–167, Feb. 2018. DOI: 10.1016/j.mechatronics.2017.12.007.

[13] Q. Feng, J. Wang, K. Kang, and F. Yang, "Study on Assist Characteristic of Commercial Vehicle EPS System Based on Lateral Acceleration," en, in *Proceedings of China SAE Congress 2020: Selected Papers*, ser. Lecture Notes in Electrical Engineering, Singapore: Springer Nature, 2022, pp. 687–701. DOI: 10.1007/978-981-16-2090-4_41.

[14] X. Guan, Y.-N. Zhang, C.-G. Duan, W.-L. Yong, and P.-P. Lu, "Study on decomposition and calculation method of EPS assist characteristic curve," en, *Proceedings of the Institution of Mechanical Engineers, Part D: Journal of Automobile Engineering*, vol. 235, no. 8, pp. 2166–2175, Jul. 2021, Publisher: IMECHE. DOI: 10.1177/0954407020987062.

[15] X. Wu, M. Zhang, and M. Xu, "Active Tracking Control for Steer-by-Wire System With Disturbance Observer," *IEEE Transactions on Vehicular Technology*, vol. 68, no. 6, pp. 5483–5493, Jun. 2019, Conference Name: IEEE Transactions on Vehicular Technology. DOI: 10.1109/TVT.2019.2910540.

[16] A. Balachandran and J. C. Gerdes, "Artificial Steering Feel Design for Steer-by-wire Vehicles," en, *IFAC Proceedings Volumes*, 7th IFAC Symposium on Advances in Automotive Control, vol. 46, no. 21, pp. 404–409, Jan. 2013. DOI: 10.3182/20130904-4-JP-2042.00131.

[17] S. Fankem and S. Müller, "A new model to compute the desired steering torque for steer-by-wire vehicles and driving simulators," en, *Vehicle System Dynamics*, vol. 52, no. sup1, pp. 251–271, May 2014. DOI: 10.1080/00423114.2014.896469.

[18] S. Fankem, T. Weiskircher, and S. Müller, "Model-based Rack Force Estimation for Electric Power Steering," en, *IFAC Proceedings Volumes*, 19th IFAC World Congress, vol. 47, no. 3, pp. 8469–8474, Jan. 2014. DOI: 10.3182/20140824-6-ZA-1003.00405.

[19] M. Mitschke and H. Wallentowitz, *Dynamik der Kraftfahrzeuge*, de. Wiesbaden: Springer Fachmedien, 2014. DOI: 10.1007/978-3-658-05068-9.

[20] D. T. McRuer and E. S. Krendel, "The human operator as a servo system element," en, *Journal of the Franklin Institute*, vol. 267, no. 5, pp. 381–403, May 1959. DOI: 10.1016/0016-0032(59)90091-2.

[21] M. Eberhart, "Theoretische Untersuchung und Entwicklung eines Fahrerassistenzsystems zur Stabilisierung des Powerslides," de, Accepted: 2022-11-03T14:38:31Z Journal Abbreviation: Theoretical investigation of the powerslide and development of a driver assist system for stabilization of the powerslide, Thesis, Wien, 2022. DOI: 10.34726/hss.2022.104000.

[22] S. Jakubek, *Grundlagen der Regelungstechnik*. Wien, Techn. Univ., 2019.

[23] M. Plöchl, *Zusammenwirken von allradgelenktem Fahrzeug und Fahrer in kritischen Fahrsituationen*, ger. Wien, Techn. Univ., Diss., 1995.

[24] J. Edelmann, *PKW-Fahrermodell für höhere Querbeschleunigungen*, ger. Wien, Techn. Univ., Dipl.-Arb., 2004.

[25] V. Schreiber, V. Ivanov, K. Augsburg, *et al.*, "Shared and Distributed X-in-the-Loop Tests for Automotive Systems: Feasibility Study," en, *IEEE Access*, vol. 6, pp. 4017–4026, 2018. DOI: 10.1109/ACCESS.2017.2789020.

[26] MathWorks, *Simulink – Simulation und Model-Based Design*. [Online]. Available: https://de.mathworks.com/products/simulink.html.

[27] Dassault Systèmes, *Simpack Multibody System Simulation Software*. [Online]. Available: https://www.3ds.com/products-services/simulia/products/simpack/.

[28] M. Kozek, S. Jakubek, and M. Stadlbauer, *Identifikation und Experimentelle Modellbildung*. Wien, Techn. Univ., 2019.

List of Figures

List of Tables

A. Appendix

A.1. Measurement of the maximum Torque

As there was no data about the maximum torque for the steering wheel Thrustmaster T300 provided, the maximum torque was measured. In the following the measurement setting is plotted.

Figure A.1.: Torque measurement setting

First, the reference value 1 is transmitted to the steering wheel, to generate the maximum torque T_{max}. The force that is needed to keep the steering wheel at 90 deg is measured with a weight scale. The maximum torque is calculated with the normal distance from the point of force application to the centre of the steering wheel (0.21 m), as follows:

$$T_{max} = 9.81 \cdot 1.89 \cdot 0.21 \approx 3.9\text{Nm}$$

Figure A.2.: Measured weight

The maximum torque is 3.9 Nm. It should be mentioned that this torque is relatively low and can be overridden by the teledriver at any point. This is an important safety aspect of the system.

A.2. Tuning Factor Set

In the following the tuning factor sets of all torque emulation modes are given. It should be noted that the tuning factor should be assigned in the specified order of the torque components:

$$\left[T_{\delta_{sw,TS}}\ T_{\dot{\delta}_{sw,TS}}\ T_{a_y}\ T_r\right]$$

	Torque components	*Tuning factor set*
Mode 0	–	[0 0 0 0]
Mode 1	$T_{\delta_{sw,TS}}$	[0.8 0 0 0]
Mode 2	$T_{\dot{\delta}_{sw,TS}}$	[0 0.18 0 0]
Mode 3	T_{a_y}	[0 0 0.15 0]
Mode 4	T_r	[0 0 0 0.15]
Mode 5	$T_{\delta_{sw,TS}}$, $T_{\dot{\delta}_{sw,TS}}$	[0.8 0.18 0 0]
Mode 6	$T_{\dot{\delta}_{sw,TS}}$, T_{a_y}	[0 0.18 0.2 0]
Mode 7	$T_{\delta_{sw,TS}}$, $T_{\dot{\delta}_{sw,TS}}$, T_{a_y}	[0.2 0.18 0.2 0]
Mode 8	$T_{\delta_{sw,TS}}$, $T_{\dot{\delta}_{sw,TS}}$, T_r	[0.3 0.18 0 0.22]
Mode 9	$T_{\delta_{sw,TS}}$, $T_{\dot{\delta}_{sw,TS}}$, T_{a_y}, T_r	[0.18 0.2 0.15 0.1]

Table A.1.: Tuning factor sets

A.3. Self-Centring

Due to the inherent friction of the telestation steering system, it may be that the self-centring tendency of the torque components $T_{\delta_{sw,TS}}$, T_{a_y}, and T_r is not sufficient to return the steering wheel to the centre position. In this case, the emulated feedback torque T can be modified to achieve self-centring. If the emulated torque is below a certain threshold, the emulated torque value is held. In the centre position, no torque is applied, but there is a greater increase of the modified feedback torque $\hat{T}$ around the

centre position until the threshold is reached. In the Figure A.3, the modified feedback torque is displayed. The dashed lines indicate the range where the feedback torque is modified. Due to the little inherent friction of the simulator steering system, this feature is not further investigated in the scope of this study.

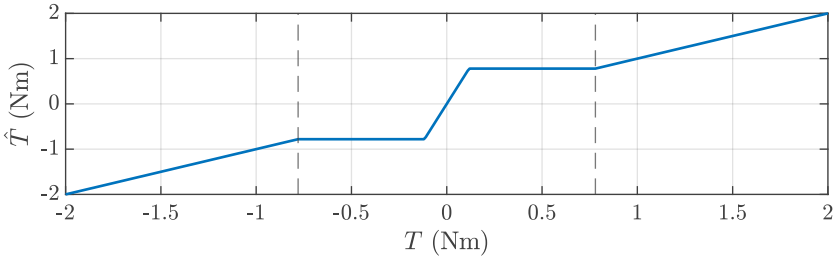

Figure A.3.: Modified feedback torque $\hat{T}$ for self-centring

A.4. Influence of the Torque Emulation on Driver 2

In this section, the reaction of Driver 2 to different torque emulation modes at different velocities is given. For a better overview, only modes 5 and 9 are compared with mode 0. It can be seen that Driver 2 handles the vehicle almost the same with and without torque feedback. Nonetheless, Driver 2's subjective feedback indicates that haptic feedback assistance enhances the steering process. Additionally, it provides the driver with valuable information about the vehicle's reaction.

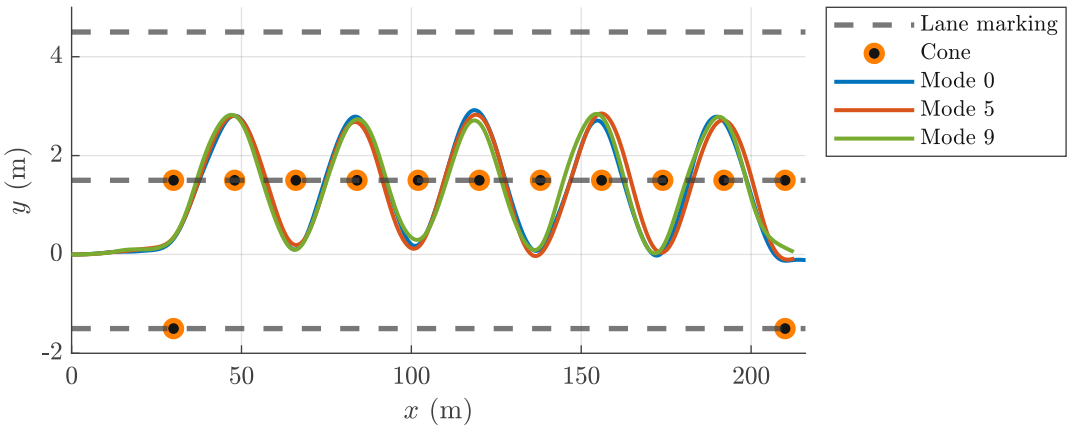

Figure A.4.: Trajectory with different torque emulation modes at $v_x = 30\,\mathrm{km/h}$ (Driver 2)

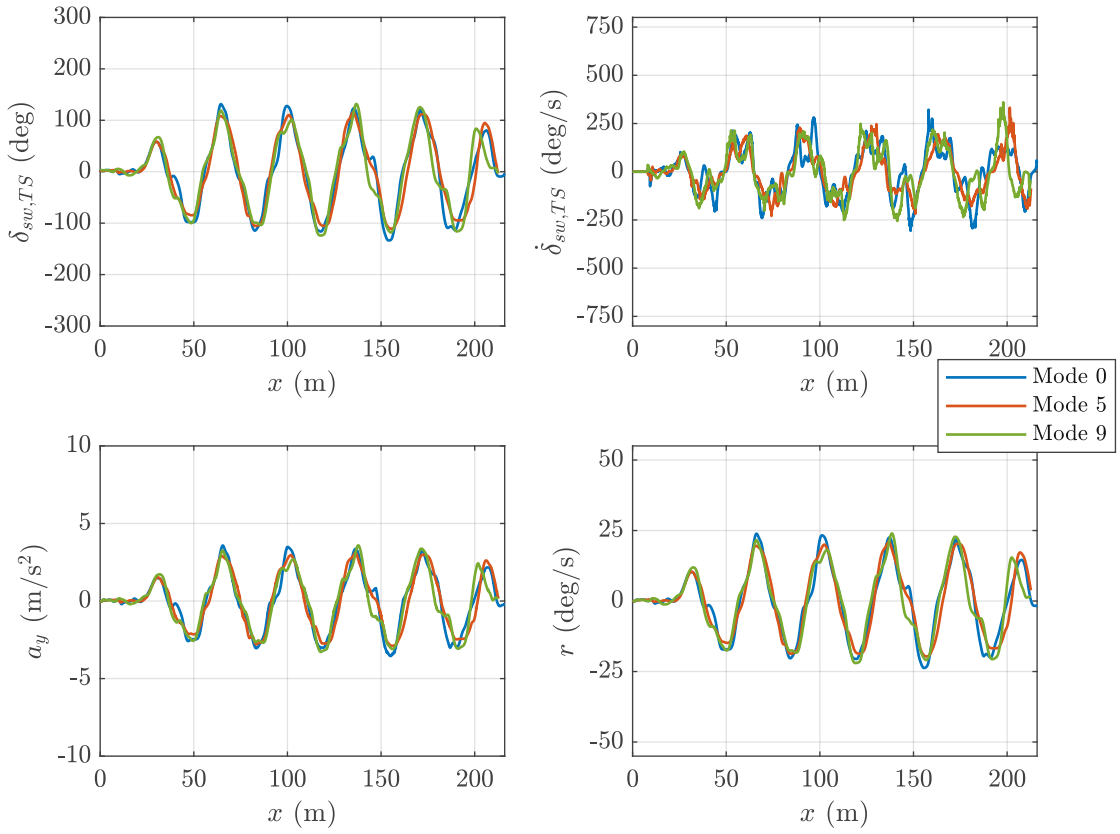

Figure A.5.: Comparison of the steering inputs and vehicle states of Driver 2 with different torque emulation modes at $v_x = 30\,\mathrm{km/h}$

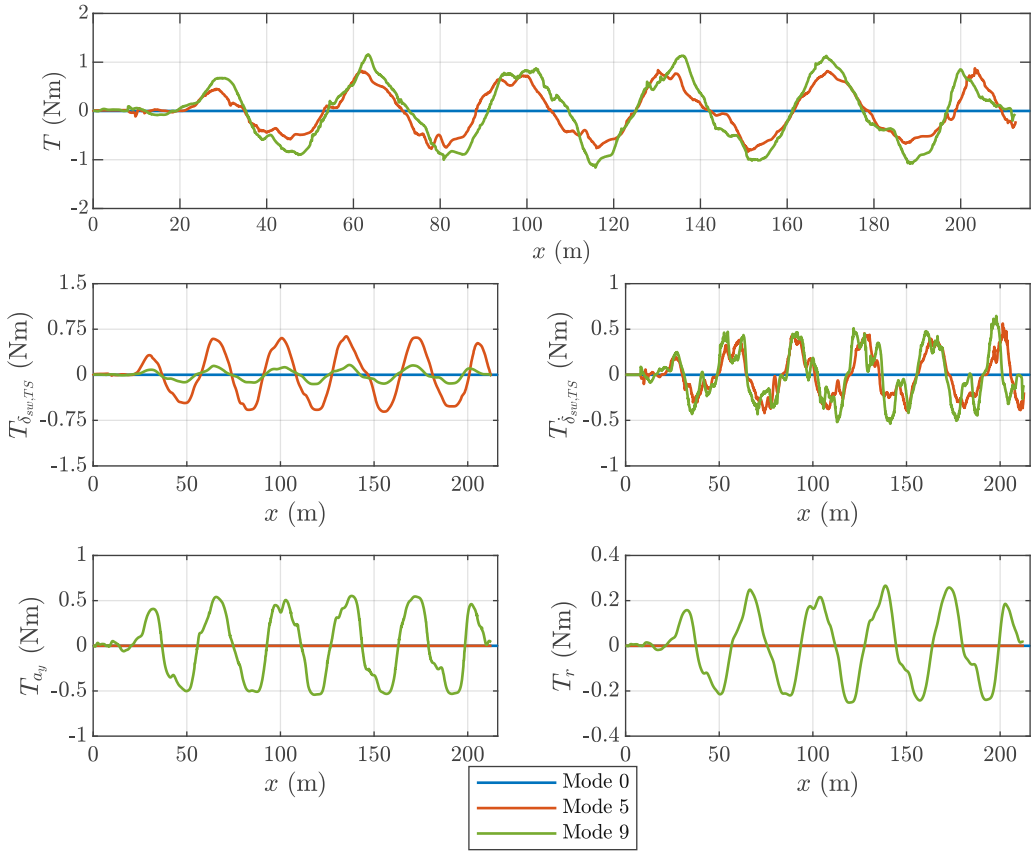

Figure A.6.: Comparison of the torque components with different torque emulation modes at $v_x = 30\,\mathrm{km/h}$ (Driver 2)

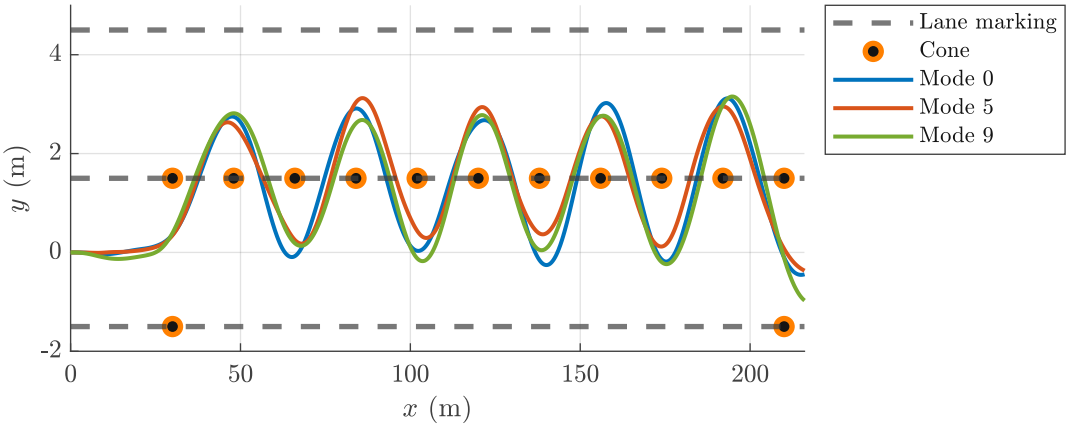

Figure A.7.: Trajectory with different torque emulation modes at $v_x = 40\,\mathrm{km/h}$ (Driver 2)

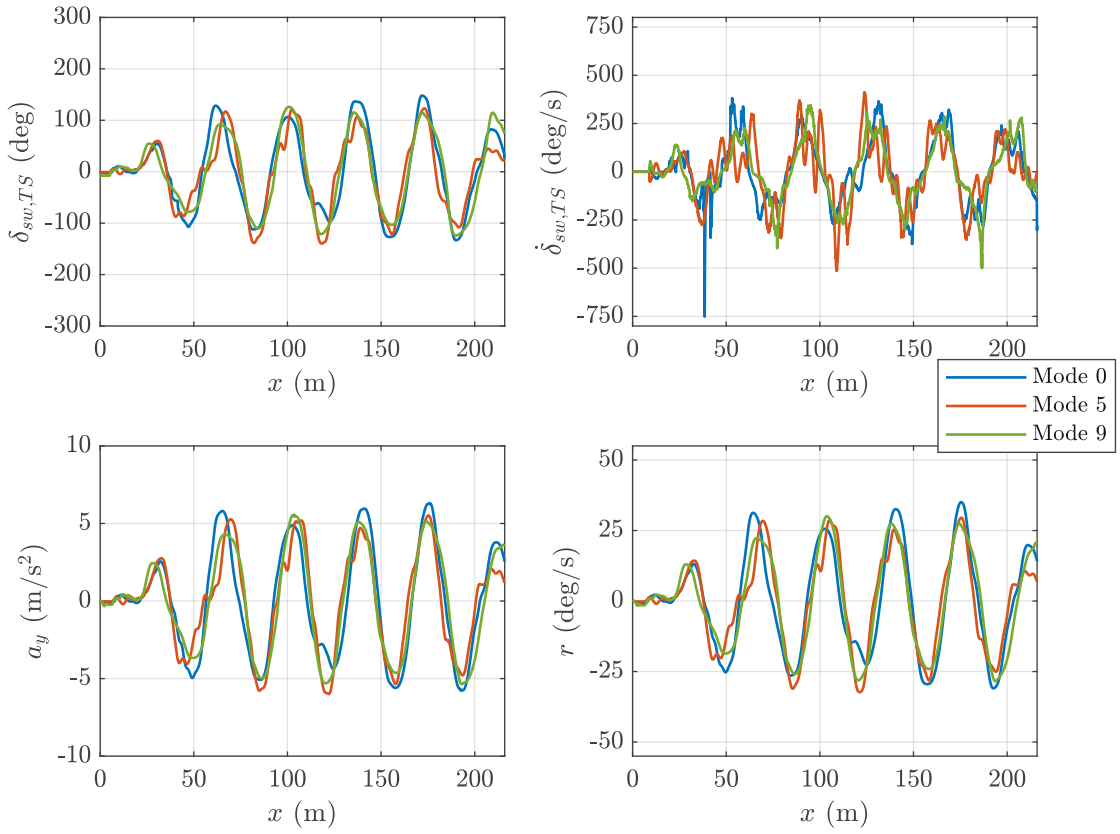

Figure A.8.: Comparison of the steering inputs and vehicle states of Driver 2 with different torque emulation modes at $v_x = 40\,\mathrm{km/h}$

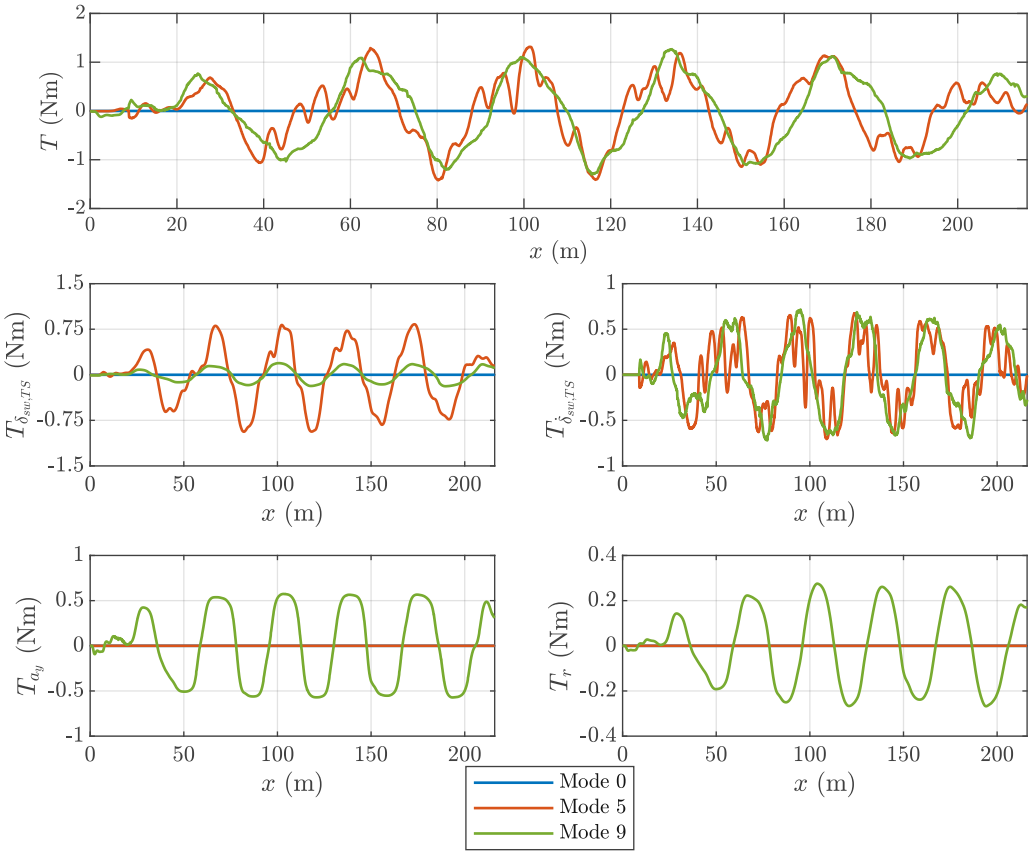

Figure A.9.: Comparison of the torque components with different torque emulation modes at $v_x = 40\,\mathrm{km/h}$ (Driver 2)